

# International Journal of Physical Sciences

Volume 10 Number 15 16 August, 2015

ISSN 1992-1950



*Academic  
Journals*

# ABOUT IJPS

The **International Journal of Physical Sciences (IJPS)** is published weekly (one volume per year) by Academic Journals.

**International Journal of Physical Sciences (IJPS)** is an open access journal that publishes high-quality solicited and unsolicited articles, in English, in all Physics and chemistry including artificial intelligence, neural processing, nuclear and particle physics, geophysics, physics in medicine and biology, plasma physics, semiconductor science and technology, wireless and optical communications, materials science, energy and fuels, environmental science and technology, combinatorial chemistry, natural products, molecular therapeutics, geochemistry, cement and concrete research, metallurgy, crystallography and computer-aided materials design. All articles published in IJPS are peer-reviewed.

## Contact Us

**Editorial Office:** [ijps@academicjournals.org](mailto:ijps@academicjournals.org)

**Help Desk:** [helpdesk@academicjournals.org](mailto:helpdesk@academicjournals.org)

**Website:** <http://www.academicjournals.org/journal/IJPS>

**Submit manuscript online** <http://ms.academicjournals.me/>

## Editors

### **Prof. Sanjay Misra**

*Department of Computer Engineering, School of Information and Communication Technology  
Federal University of Technology, Minna,  
Nigeria.*

### **Prof. Songjun Li**

*School of Materials Science and Engineering,  
Jiangsu University,  
Zhenjiang,  
China*

### **Dr. G. Suresh Kumar**

*Senior Scientist and Head Biophysical Chemistry  
Division Indian Institute of Chemical Biology  
(IICB)(CSIR, Govt. of India),  
Kolkata 700 032,  
INDIA.*

### **Dr. Remi Adewumi Oluyinka**

*Senior Lecturer,  
School of Computer Science  
Westville Campus  
University of KwaZulu-Natal  
Private Bag X54001  
Durban 4000  
South Africa.*

### **Prof. Hyo Choi**

*Graduate School  
Gangneung-Wonju National University  
Gangneung,  
Gangwondo 210-702, Korea*

### **Prof. Kui Yu Zhang**

*Laboratoire de Microscopies et d'Etude de  
Nanostructures (LMEN)  
Département de Physique, Université de Reims,  
B.P. 1039. 51687,  
Reims cedex,  
France.*

### **Prof. R. Vittal**

*Research Professor,  
Department of Chemistry and Molecular  
Engineering  
Korea University, Seoul 136-701,  
Korea.*

### **Prof Mohamed Bououdina**

*Director of the Nanotechnology Centre  
University of Bahrain  
PO Box 32038,  
Kingdom of Bahrain*

### **Prof. Geoffrey Mitchell**

*School of Mathematics,  
Meteorology and Physics  
Centre for Advanced Microscopy  
University of Reading Whiteknights,  
Reading RG6 6AF  
United Kingdom.*

### **Prof. Xiao-Li Yang**

*School of Civil Engineering,  
Central South University,  
Hunan 410075,  
China*

### **Dr. Sushil Kumar**

*Geophysics Group,  
Wadia Institute of Himalayan Geology,  
P.B. No. 74 Dehra Dun - 248001(UC)  
India.*

### **Prof. Suleyman KORKUT**

*Duzce University  
Faculty of Forestry  
Department of Forest Industrial Engineering  
Beciyorukler Campus 81620  
Duzce-Turkey*

### **Prof. Nazmul Islam**

*Department of Basic Sciences &  
Humanities/Chemistry,  
Techno Global-Balurghat, Mangalpur, Near District  
Jail P.O: Beltalpark, P.S: Balurghat, Dist.: South  
Dinajpur,  
Pin: 733103,India.*

### **Prof. Dr. Ismail Musirin**

*Centre for Electrical Power Engineering Studies  
(CEPES), Faculty of Electrical Engineering, Universiti  
Teknologi Mara,  
40450 Shah Alam,  
Selangor, Malaysia*

### **Prof. Mohamed A. Amr**

*Nuclear Physic Department, Atomic Energy Authority  
Cairo 13759,  
Egypt.*

### **Dr. Armin Shams**

*Artificial Intelligence Group,  
Computer Science Department,  
The University of Manchester.*

## Editorial Board

**Prof. Salah M. El-Sayed**

*Mathematics. Department of Scientific Computing,  
Faculty of Computers and Informatics,  
Benha University. Benha ,  
Egypt.*

**Dr. Rowdra Ghatak**

*Associate Professor  
Electronics and Communication Engineering Dept.,  
National Institute of Technology Durgapur  
Durgapur West Bengal*

**Prof. Fong-Gong Wu**

*College of Planning and Design, National Cheng Kung  
University  
Taiwan*

**Dr. Abha Mishra.**

*Senior Research Specialist & Affiliated Faculty.  
Thailand*

**Dr. Madad Khan**

*Head  
Department of Mathematics  
COMSATS University of Science and Technology  
Abbottabad, Pakistan*

**Prof. Yuan-Shyi Peter Chiu**

*Department of Industrial Engineering & Management  
Chaoyang University of Technology  
Taichung, Taiwan*

**Dr. M. R. Pahlavani,**

*Head, Department of Nuclear physics,  
Mazandaran University,  
Babolsar-Iran*

**Dr. Subir Das,**

*Department of Applied Mathematics,  
Institute of Technology, Banaras Hindu University,  
Varanasi*

**Dr. Anna Oleksy**

*Department of Chemistry  
University of Gothenburg  
Gothenburg,  
Sweden*

**Prof. Gin-Rong Liu,**

*Center for Space and Remote Sensing Research  
National Central University, Chung-Li,  
Taiwan 32001*

**Prof. Mohammed H. T. Qari**

*Department of Structural geology and remote sensing  
Faculty of Earth Sciences  
King Abdulaziz UniversityJeddah,  
Saudi Arabia*

**Dr. Jyhwen Wang,**

*Department of Engineering Technology and Industrial  
Distribution  
Department of Mechanical Engineering  
Texas A&M University  
College Station,*

**Prof. N. V. Sastry**

*Department of Chemistry  
Sardar Patel University  
Vallabh Vidyanagar  
Gujarat, India*

**Dr. Edilson Feredna**

*Graduate Program on Knowledge Management and IT,  
Catholic University of Brasilia,  
Brazil*

**Dr. F. H. Chang**

*Department of Leisure, Recreation and Tourism  
Management,  
Tzu Hui Institute of Technology, Pingtung 926,  
Taiwan (R.O.C.)*

**Prof. Annapurna P.Patil,**

*Department of Computer Science and Engineering,  
M.S. Ramaiah Institute of Technology, Bangalore-54,  
India.*

**Dr. Ricardo Martinho**

*Department of Informatics Engineering, School of  
Technology and Management, Polytechnic Institute of  
Leiria, Rua General Norton de Matos, Apartado 4133, 2411-  
901 Leiria,  
Portugal.*

**Dr Driss Miloud**

*University of mascara / Algeria  
Laboratory of Sciences and Technology of Water  
Faculty of Sciences and the Technology  
Department of Science and Technology  
Algeria*

**Prof. Bidyut Saha,**

*Chemistry Department, Burdwan University, WB,  
India*

**ARTICLES**

<b>Hydrogeophysical study of aquifer characteristics in some parts of Nsukka and Igbo Eze south local government areas of Enugu State, Nigeria</b>	<b>425</b>
Maximus C. Ugwuanyi, Johnson C. Ibuot and Daniel N. Obiora	
<b>Electrical conductivity and uniaxial shear tests on soil samples</b>	<b>436</b>
Tekin Yeken	
<b>General Relativity support from the double pulsar</b>	<b>456</b>
Keith John Treschman	

*Full Length Research Paper*

## Hydrogeophysical study of aquifer characteristics in some parts of Nsukka and Igbo Eze south local government areas of Enugu State, Nigeria

Maximus C. Ugwuanyi, Johnson C. Ibuot and Daniel N. Obiora\*

Department of Physics and Astronomy, University of Nigeria, Nsukka, Enugu State, Nigeria.

Received 4 June, 2015; Accepted 27 July, 2015

Resistivity survey was carried out in some parts of Nsukka and Igbo Eze south local government areas of Enugu State, in order to evaluate the groundwater conditions of the area. The area is devoid of surface water and lack of proper knowledge of the aquifer has affected the extraction and development of groundwater in the area since it is the major source of water. Resistivity, thickness, depth, curve frequencies and Dar-Zarrouk parameters were determined. The result revealed a total of three to five geoelectric layers with the range of resistivity and thickness values as; topmost layer: 121.6 - 2155.3  $\Omega\text{m}$  and 0.9 - 3.6 m; second layer: 794.4 - 4823.5  $\Omega\text{m}$  and 5.2 - 24.0 m; third layer: 1226.6 - 4703.1  $\Omega\text{m}$  and 29.3 - 175.0 m; fourth layer: 4261.2 - 20998.8  $\Omega\text{m}$  and the fifth layer is undefined in most of the vertical electrical sounding (VES) stations. The Dar-Zarrouk parameters computed show the longitudinal conductance to range from 0.01 - 0.09 mhos with a mean value of 0.029 mhos. The curve types obtained from the study were; KH, H, AA, KHA, AAA. The transverse resistance ranges from 17048.82 - 863269.68  $\Omega\text{m}^2$  with 271805  $\Omega\text{m}^2$  as the mean value. The aquifer layers show resistivity range of 1226.6 - 7087.6  $\Omega\text{m}$  with thickness range of 13.4 - 175.0 m and are composed mainly of sandstone. The contour maps drawn show the variation of aquifer parameters and Dar-Zarrouk parameters. The study area was generally delineated as having a poor protective capacity as a result of the low values of longitudinal conductance of the aquiferous layers, but high transmissivity and permeability which suggest high groundwater potential.

**Key words:** Groundwater conditions, Nsukka and Igbo Eze south, protective capacity, transmissivity, permeability, aquiferous layers.

### INTRODUCTION

Shortage of water supply and difficulty in drilling of groundwater has been prevalent in Nsukka and Igbo Eze South local government areas of Enugu State. The residents of Nsukka and Igbo-Eze South local

government areas are always faced with the condition of acute water scarcity. This condition can be sometimes so severe especially during the dry season. This area is devoid of surface water (stream, rivers, ponds and lakes).

\*Corresponding author. E-mail: [daniel.obiora@unn.edu.ng](mailto:daniel.obiora@unn.edu.ng), Tel: +2348038804735.

Author(s) agree that this article remain permanently open access under the terms of the [Creative Commons Attribution License 4.0 International License](https://creativecommons.org/licenses/by/4.0/)

Hence the residents depend solely on borehole water for their domestic, industrial and agricultural purposes. There are, however, few scattered boreholes within this area. Some did not function from onset, while some had failed. The development of groundwater in this area is constrained by lack of knowledge of the aquiferous nature of the subsurface geomaterials, which is necessary for borehole construction. Groundwater represents part of the subsurface water occurring in the zone of saturation (phreatic zone) below the water table. According to Plummer (2000), the source of groundwater is rainfall and snowbelt. In prospecting for groundwater, or looking for good site to drill water wells, a certain favourable geologic material called aquifer is sought for. These favourable materials are sedimentary deposits or rocks that are sufficiently permeable to transmit economically significant quantities of water. The nature of the aquifer is a function of subsurface geological composition that play an important role in determining the circulation of water from the surface (infiltration) to subsurface water through recharge processes (Bashir et al., 2014).

Groundwater generally requires no prior treatment since it is naturally protected from contamination. It does not vary significantly seasonally and is often drought resistant. It lends itself to the principles of community management- it can be found close to the point of demand and be developed incrementally (McDonald et al., 2005). The sluggish flow through small voids helps in purifying groundwater, necessitating lower or no treatment costs prior to its use as drinking water (Onugba and Yaya, 2008).

There is a need for geophysical study in this area so as to solve the problem of abortive boreholes for effective groundwater exploration, exploitation and management. Many researchers have carried out resistivity survey to locate the prospect and potential groundwater zones for exploration in order to achieve long term sustainability (Okolie, 2013; George et al., 2011; Okpara et al., 2012; Ezeh et al., 2013; Lashkaripour, 2003; Ibuot et al., 2013). Resistivity method has successfully been employed in geological terrains to delineate subsurface geological structures, aquifer units, types, thickness and depth extent of area of study. It is used because of the correlation that exists between electrical properties, geologic formations and fluid contents. In groundwater exploration, the vertical electrical sounding (VES) technique is commonly used due to its simplicity to determine the variation of the subsurface geomaterials. According to Todd (2004), electrical resistivity of most rocks depends on the amount of water in their pores, distribution of these pores and the salinity of the water. This research paper attempts to identify prospective groundwater potential zones and evaluate the aquifer characteristics in terms of the availability of groundwater for groundwater development in Nsukka and Igbo Eze South local government areas.

## LOCATION AND GEOLOGY OF THE STUDY AREA

The study area is located within latitudes 6°52'N and 6°58'N and longitudes 7°20'E and 7°27'E. It covers an area extent of about 20.825 km<sup>2</sup> in Nsukka and Igbo-Eze South local government areas (L. G. A) of Enugu State. It covers Obukpa and parts of Alor-uno in Nsukka L.G.A, and parts of Ibagwa-aka and Iheakpu-awka in Igbo-Eze South L.G.A. The region has an undulating topography and the elevation varies between 359 and 413 m above sea level (Figure 1). These areas of study are accessible through a network of major and minor roads in addition to several foot paths. The study area is found within the Anambra sedimentary basin whose rocks are the Upper Cretaceous in age. The geologic formations are the upper Nsukka Formation and the underlying Ajali Sandstone. The major land forms typical of this area are the residual hills and dry valleys. These two major geomorphic structures are the resultant effect of weathering and differential erosion of clastic materials which are remnant of Nsukka Formation. Ofomata (1967) recognized five types of these residual hills according to their shapes. These residual hills sometimes form outliers on the Ajali Sandstone and are capped by thick deposit of red earthy material and laterite. These laterites are permeable, particularly those of Ajali sandstone thereby allowing easy water percolation into the groundwater table during the rainy season. The Ajali Sandstone consists mainly of medium to coarse grained characteristically white coloured sandstone but may be occasionally iron stained. The sandstone is very permeable and readily recharged in its outcrop belt around the Idah-Nsukka-Enugu escarpment (Agagu et al., 1985). Nsukka formation has a significant groundwater potential and hosts a number of low to moderate yield wells in Nsukka areas. A number of perched aquifer emerges from it and quite a number of low yield wells also tap the perched aquifer in Nsukka areas (Ezeigbo and Ozioko, 1987). The laterite capping in the area is aquiferous due to their vesicular nature, hence it is porous and permeable. These lateritic caps may be underlain by a less pervious clay beds leading to the formation of perched aquifer in some areas. Perched aquifer discharge is seen in Asho hill in Nsukka, Aku hill in Obukpa, Abile hill in Ibagwa-aka and Awula in Ibagwa-Ani. In many areas however, the laterite cap has been washed out and the clay bed underlying is missing, hence perched aquifer does not form. The sandstone members have a permeability of 2.0 – 20.7 x 10<sup>-10</sup> cm/s (Mamah and Ekine, 1989).

## MATERIALS AND METHODS

The resistivity data was acquired by vertical electrical sounding (VES) employing the Schlumberger array with maximum electrode separation of 800 m. This was done using a signal averaging system branded ABEM SAS 300 Terrameter and accessories. The

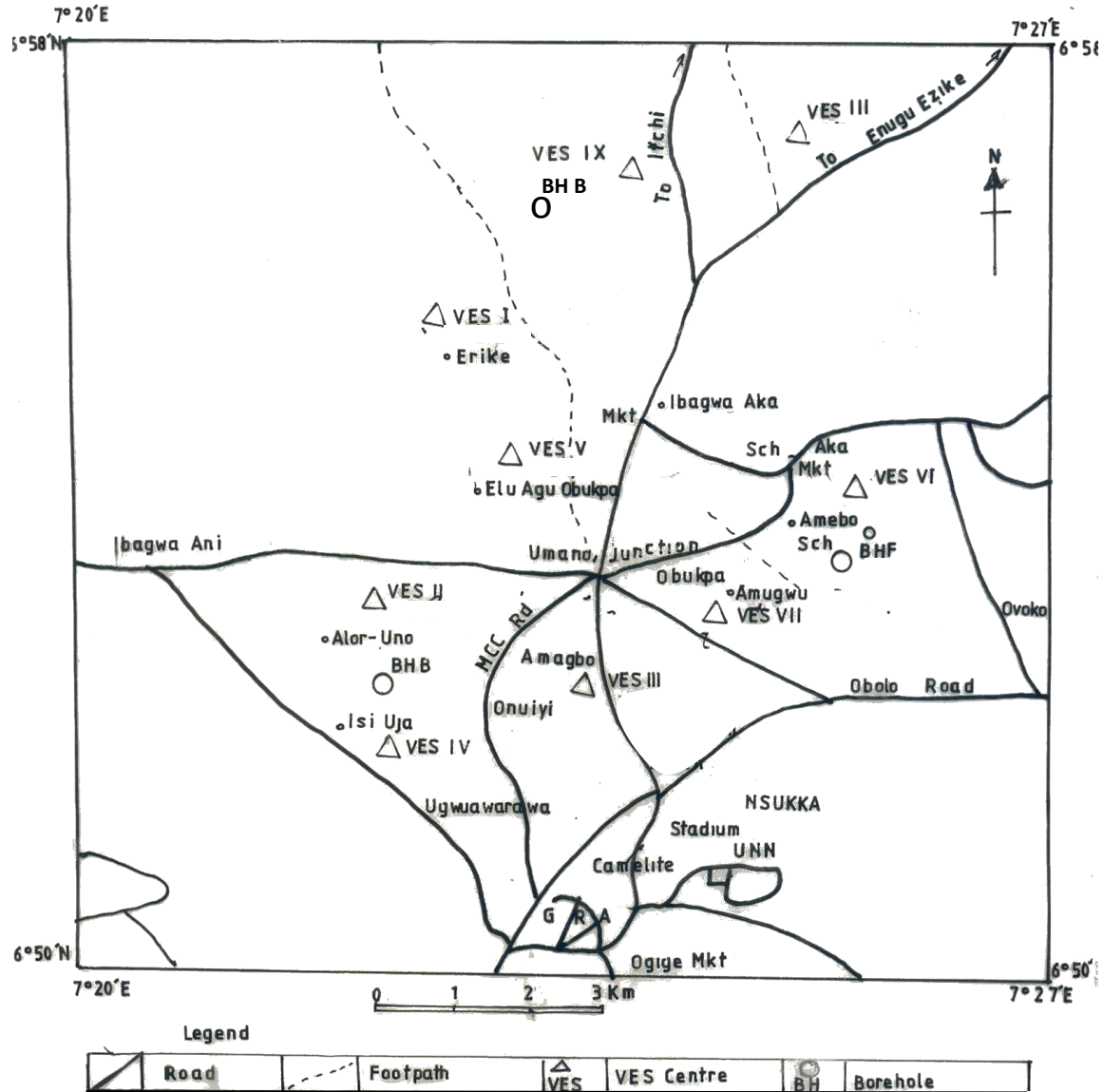


Figure 1. Location map of the study area showing the VES stations.

survey was completed with nine sounding stations. The half potential and current electrode separations were  $AB/2$  of 1.5 to 500 m and  $MN/2$  of 0.5 to 42 m. The coordinates (latitude and longitude) were measured using the Global Positioning System (GPS). The lithology information from drilled borehole was used to constrain the processed apparent resistivity. These were boreholes close to VES 6 and 9 (Figure 2). Field curves for the nine sounding stations were obtained by plotting the apparent resistivity against half-current electrode separation  $AB/2$  using a bi-logarithm graph.

A WinResist software was used to improve on that, generate a data set for the estimated model and to reduce the geoelectrical sounding curves in terms of resistivity, thickness and depth of each geoelectric layers. The resistivity model curves for some of the VES stations are shown in Figures 3 to 5. The resistivity and thickness are used to calculate the longitudinal conductance (S) and transverse resistance (R) which are known as the Dar-Zarrouk

parameters. These parameters help in evaluating the protective capacity and transmissivity of the aquifer layers (Maillet, 1947; Niwas and Singhal, 1981; Mbonu et al., 1991). These parameters are given as:

$$S = \frac{h}{\rho} \tag{1}$$

$$R = \rho h \tag{2}$$

Where  $\rho$  and  $h$  are the layers resistivity and thickness respectively. For clean saturated aquifers whose natural fluid characteristics are fairly constant, the hydraulic conductivity is proportional to the resistivity of the aquifer (Mbonu et al., 1991). Hence, the aquifer hydraulic conductivity  $K$  can be approximated to the true resistivity of the aquifer in the absence of pumping test (Hubbard and Robin, 2005).



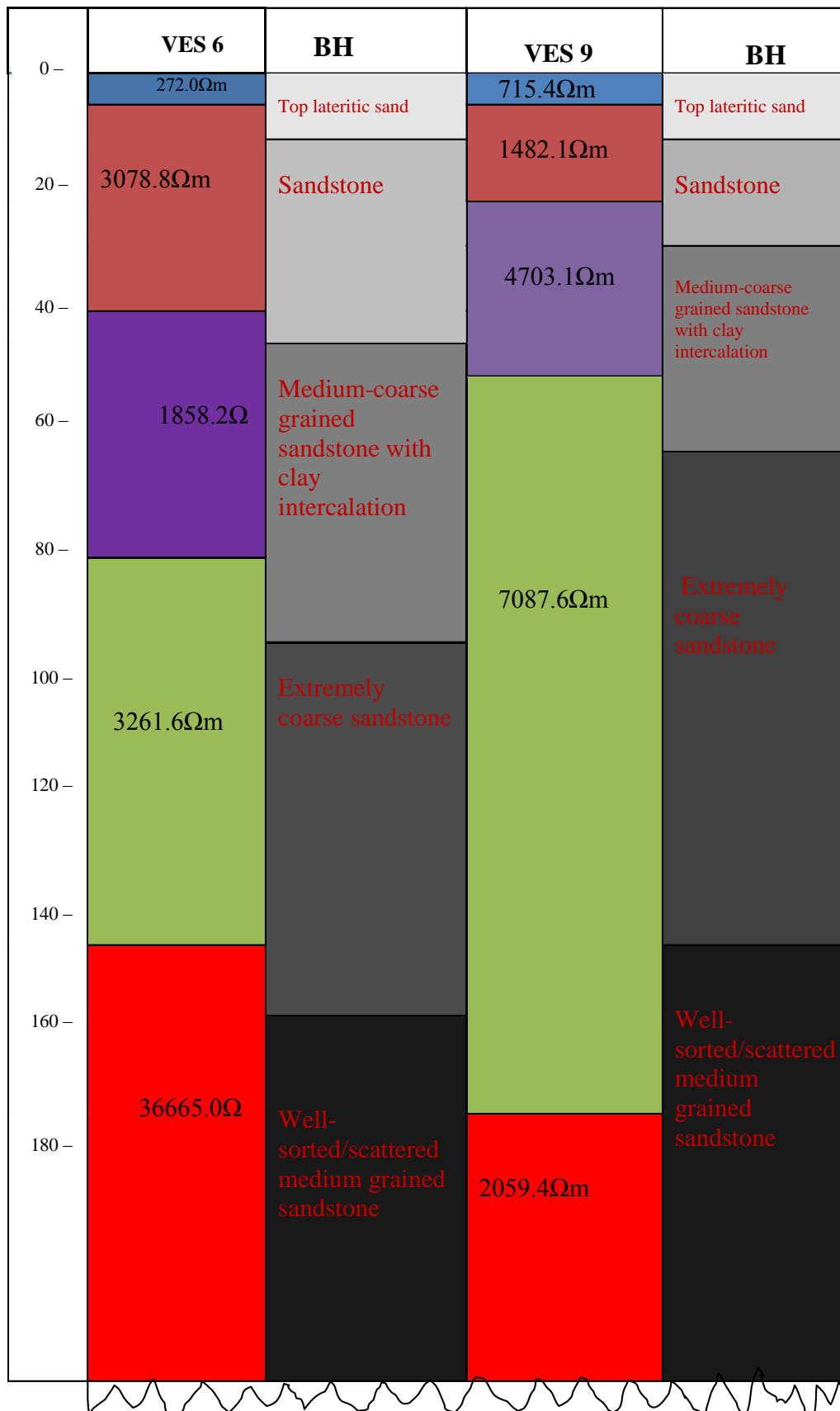


Figure 2. Lithology log of drilled boreholes close to VES 6 and 9.

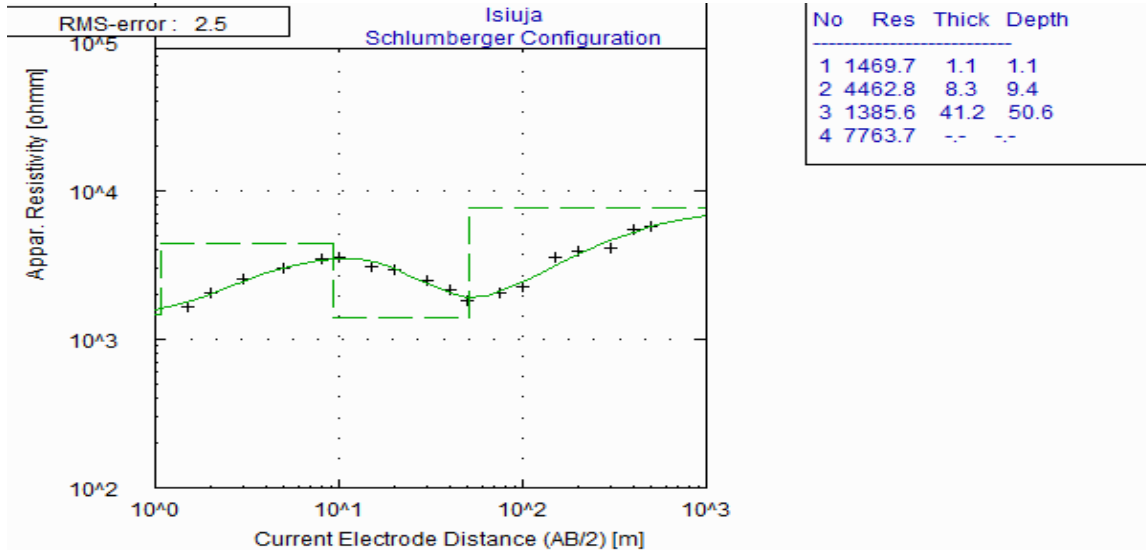


Figure 3. Typical VES curve for Isuija (VES 4).

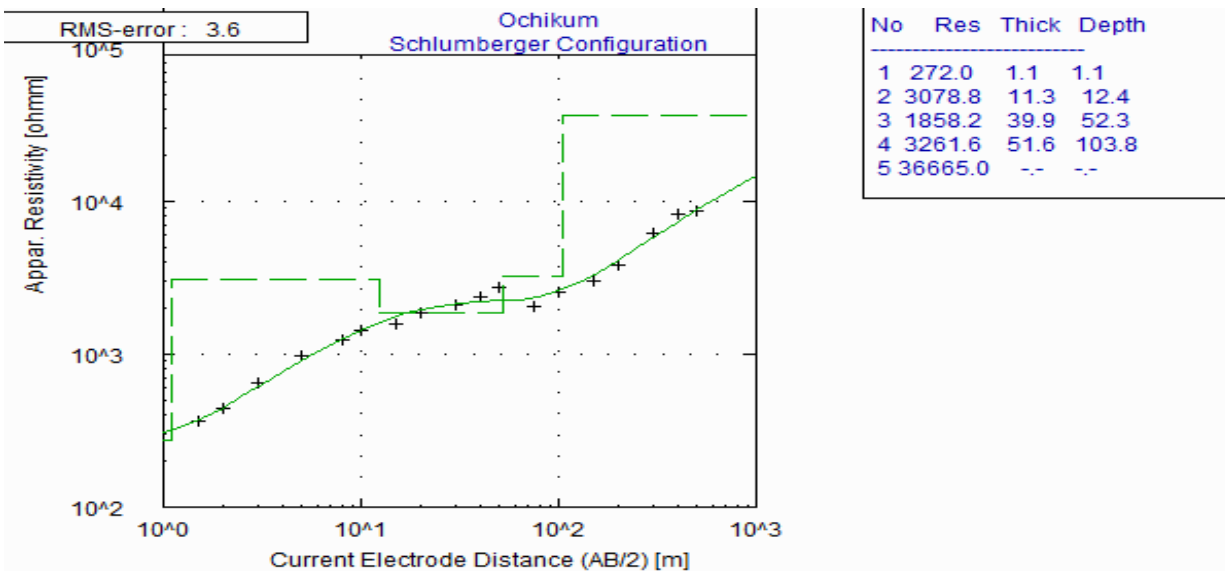


Figure 4. Typical VES curve for Ochikum (VES 6).

$$T = Kh = \rho h \tag{3}$$

Since,  $R = \rho h$ , then numerically

$$T = R \tag{4}$$

### RESULTS AND DISCUSSION

The results of the VES data from the computer modeling

are presented in Table 1. The results show a geoelectric stratification of three to five layers with the following observed curve types: KH, H, AA, KHA, AAA with KH as the dominant curve type. The topmost layer whose resistivity values range from 121.6- 2155.3  $\Omega$ m has thickness values ranging from 0.9 - 3.6 m. This layer can be said to be dominated by lateritic sand. Underlain the topsoil is a more resistive layer with resistivity range of 794.4 - 4823.5  $\Omega$ m and thickness range of 5.2 - 24.0 m. This layer lithology is mostly sandstone. The third layer which harbours most of the aquifers in the study area has a resistivity range of 1226.6 - 4703.1  $\Omega$ m and thickness

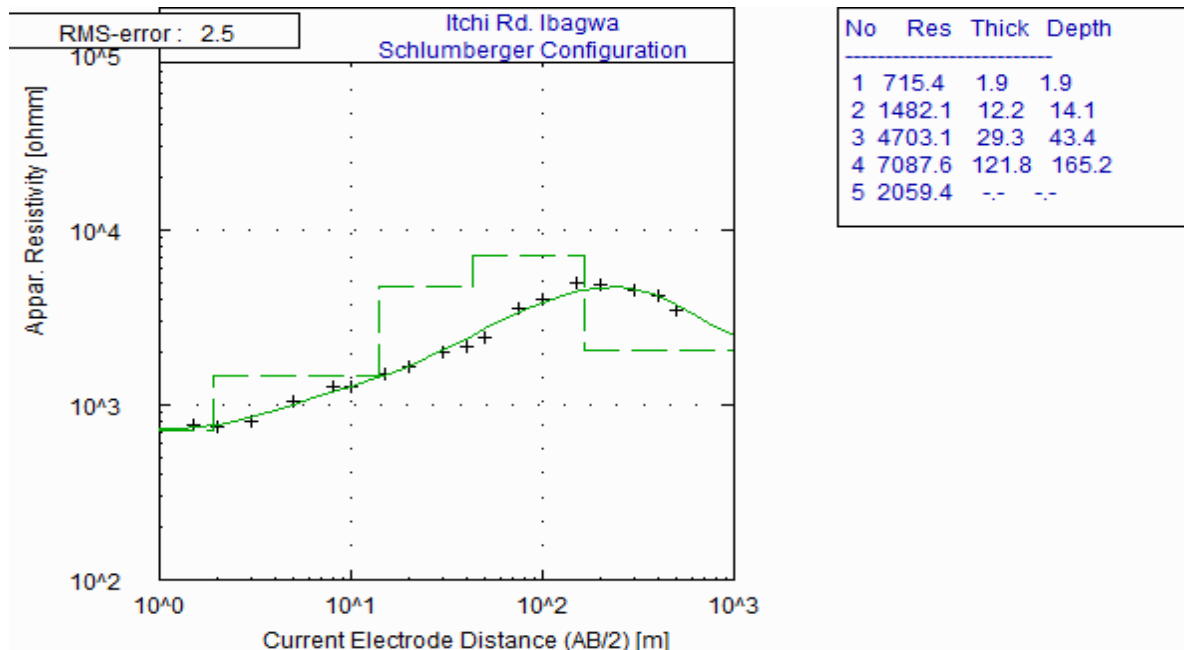


Figure 5. Typical VES curve for Itchi Road, Ibagwa-Ani (VES 9).

range of 29.3 - 175.0 m. This layer is relatively thick compared to the other layers and is said to compose of medium-coarse grained sandstone with clay intercalation. The fourth layer is highly resistive having a range of resistivity of 4261.2 - 20998.8  $\Omega\text{m}$  and undefined thickness in most of the VES stations. This layer has an extremely coarse sandstone lithology. The fifth layer is undefined in most of the VES stations within the maximum current penetration.

Table 2 shows the computed Dar-zarrouk parameters and the coordinates of each of the sounding stations. The aquifer resistivity ranges from 1226.6 - 7087.6  $\Omega\text{m}$  with thickness range of 13.4 - 175.0 m. The mean aquifer resistivity and thickness are 3024.6  $\Omega\text{m}$  and 73.99 m respectively. The longitudinal conductance computed from the aquifer resistivity and thickness has range of 0.01 - 0.09 mhos with a mean value of 0.029 mhos and the transverse resistance ranges from 17048.82 - 863269.68  $\Omega\text{m}^2$  with a mean value of 271805.1  $\Omega\text{m}^2$ . Figure 6 is a contour map of resistivity distribution of the topmost layer. The resistivity of the first layer increases from the eastern part of the study area towards the western part. This implies that the western part of the study area will have highly conductive geomaterials. Aquifer resistivity is observed to be high in the eastern part while the northern part (northeast - northwest) have low aquifer resistivity (Figure 7). Resistivity of layers depends more on the saturation of the layers and not necessarily on the thickness of the aquifer. Hence higher resistivities may not correlate with areas of thicker aquifer.

Figure 8a and b are contour maps showing the

variation of the thickness of the aquifer layer. High thickness is observed in the south-western part and decreases towards the north-eastern part of the study area. From Table 2, it can be deduced that the protective capacity of the study area is generally poor (longitudinal conductance value < 0.1). The contour map (Figure 9) shows that it decreases from west to east of the study area. It can be inferred based on the low values of longitudinal conductance that the study area is not underlain by thick layers of conducting sediments and also the presence of high percentage of conducting clays. Transmissivity of an aquifer is assumed to be controlled by the thickness of the specific layer and the presence of fine/clay particles (Utom et al., 2012). The central part of the study area has the highest transmissivity due to high transverse resistance values and the northern part is observed to have lower transmissivity (Figure 10). It can be inferred that the transmissivity and permeability in the central part will be very high. It is evident that higher transmissivities are expected in the areas underlain by the Ajali formation (Ezeh and Ukwu, 2010). This is due to the high permeability of the Ajali sandstone. Thus, the low protective capacity of the aquiferous layer and high transmissivities will support the seepage of contaminant loads and migration within the groundwater aquifer system. Groundwater potential of the study area is classified into good and moderate groundwater zones using the aquifer thickness. Zones with aquifer thickness >25 m with low clay content are zones with high groundwater potential which is about 88% of the study area, while zone with thickness ranging between 10-25 m will have moderate groundwater potential with moderate

**Table 1.** Summary of results from computer modelling for nine sounding stations.

VES No	Location	No of layers	Curve types	Layer Resistivity ( $\Omega m$ )					Thickness (m)					Depth (m)				
				$\rho_1$	$\rho_2$	$\rho_3$	$\rho_4$	$\rho_5$	$h_1$	$h_2$	$h_3$	$h_4$	$h_5$	$d_1$	$d_2$	$d_3$	$d_4$	$d_5$
1	Erike	4	KH	1022.9	1391.1	3332.4	16034.4	-	3.6	24.0	81.3	-	-	3.6	27.7	109.0	-	-
2	Alor-uno	3	H	2155.3	1272.3	2836.1	-	-	2.9	13.4	-	-	-	2.9	16.2	-	-	-
3	Amaogbo	4	KH	772.2	4823.5	1436.9	20998.8	-	0.9	9.2	34.1	-	-	0.9	9.2	34.1	-	-
4	Isuija	4	KH	1469.7	4462.8	1385.6	7763.7	-	1.1	8.3	41.2	-	-	1.1	9.4	50.6	-	-
5	Eluagu	4	AA	127.0	794.4	4107.1	18144.4	-	0.9	16.7	175.0	-	-	0.9	17.6	192.6	-	-
6	Ochikum	5	KHA	272.0	3078.8	1858.2	3261.6	366665.0	1.1	11.3	39.9	51.6	-	1.1	12.4	52.3	103.8	-
7	Amaugwu	4	KH	121.6	1989.4	1226.6	4261.2	-	3.2	5.2	114.1	-	-	3.2	8.4	122.5	-	-
8	Ibagwa	4	AA	489.4	1442.3	4111.3	7517.2	-	1.0	16.6	42.6	-	-	1.0	17.6	60.3	-	-
9	Itchi Rd Ibagwa	5	AAA	715.4	1482.1	4703.1	7087.6	2059.4	1.9	12.2	29.3	121.8	-	1.9	14.1	43.4	165.2	-

**Table 2.** Computed aquifer and Dar-zarrouk parameters from the VES result.

VES No	Location	Longitude ( $^{\circ}E$ )	Latitude ( $^{\circ}N$ )	Aquifer resistivity ( $\Omega m$ )	Aquifer thickness (m)	Longitudinal conductance (mhos)	Transverse resistance ( $\Omega m^2$ )
1	Erike	7.2633	6.5167	3332.4	81.3	0.02	270924.12
2	Alor-Uno	7.2667	6.5633	1272.3	13.4	0.01	17048.82
3	Amaogbo	7.2533	6.5767	1436.9	24.9	0.02	35778.81
4	Isuija	7.2438	6.5582	1385.6	41.2	0.03	57086.72
5	Eluagu	7.2400	6.5387	4107.1	175.0	0.04	718742.50
6	Ochikum	7.2615	6.5712	3261.6	51.6	0.02	168298.56
7	Amaugwu	7.2286	6.5646	1226.6	114.1	0.09	139955.06
8	Ibagwa	7.2377	6.5783	4111.3	42.6	0.01	175141.38
9	Itchi Rd. Ibagwa	7.2549	6.5497	7087.6	121.8	0.02	863269.68

clay content and that is obtainable in Amaogbo. It can be inferred that groundwater potential will be good since the transverse resistance, resistivity and thickness of the aquifer are high and also likely have high transmissivity. This will be suitable for development of boreholes for potable water supply. A good borehole in the study area

should be drilled to a depth within the third and fourth layer.

**Conclusion**

The present study has helped in evaluating the

groundwater conditions of the study area. The vertical electrical sounding was applied and the result was useful in delineating different geoelectric layers. The topmost layer was revealed to be lateritic sand. The lithology of the underlain layers was delineated to compose mainly of sandstone with clay intercalation. It can

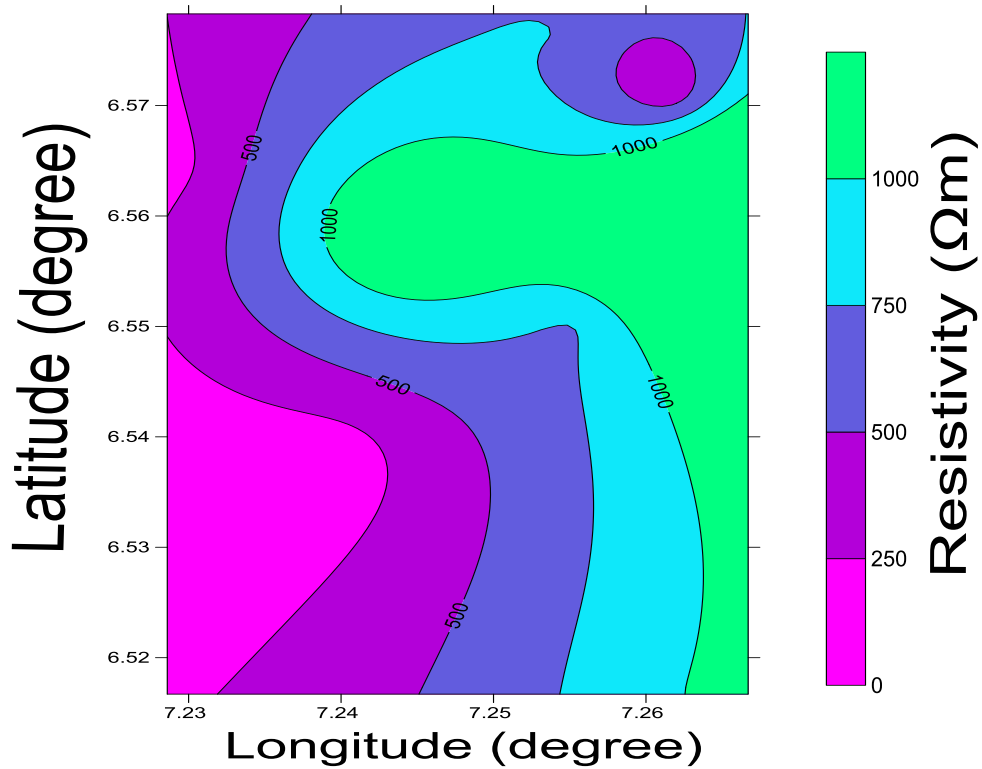


Figure 6. Contour map showing the distribution of topmost layer resistivity.

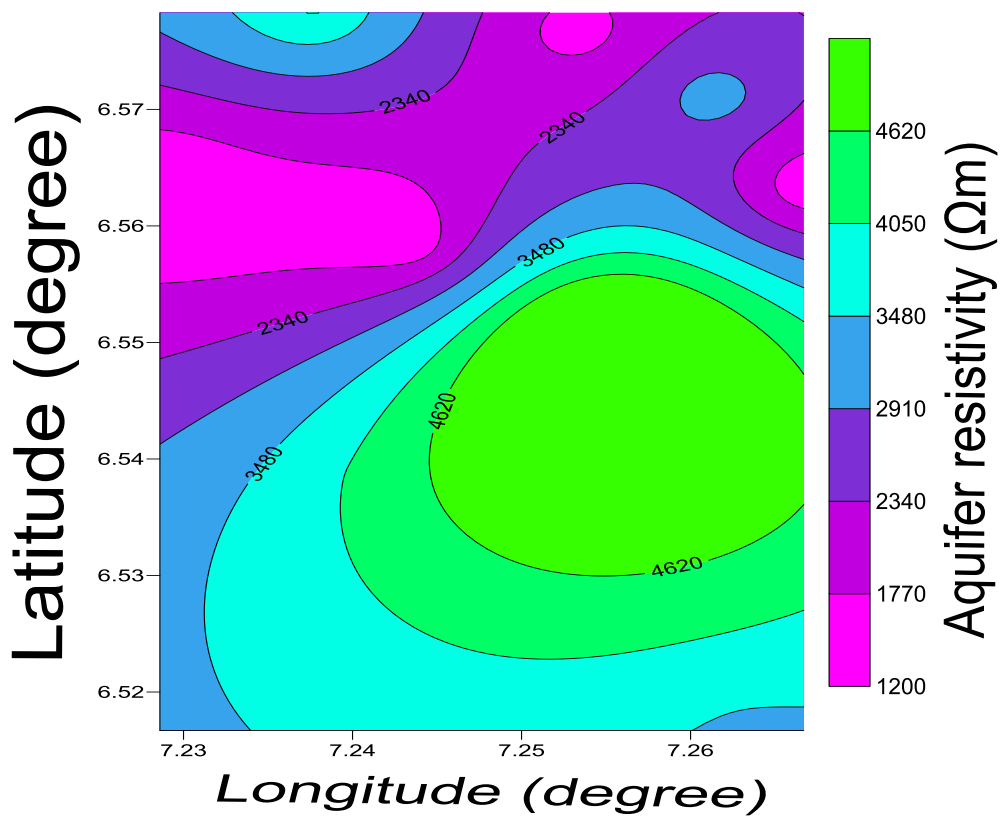


Figure 7. Contour map showing the variation of aquifer resistivity.

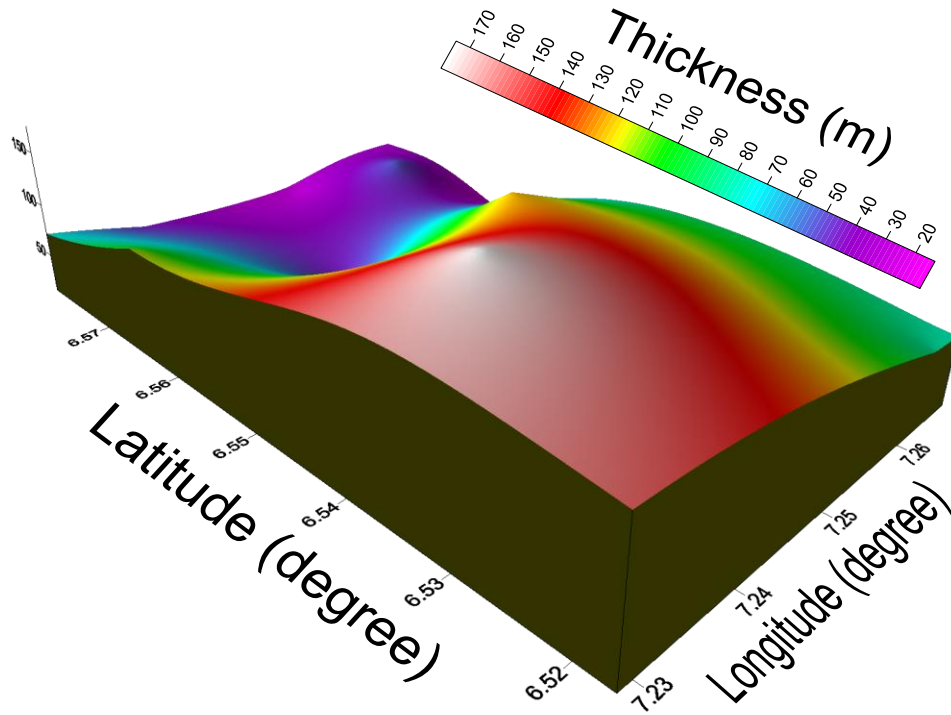


Figure 8a. A 3-D contour map showing the distribution of aquifer resistivity.

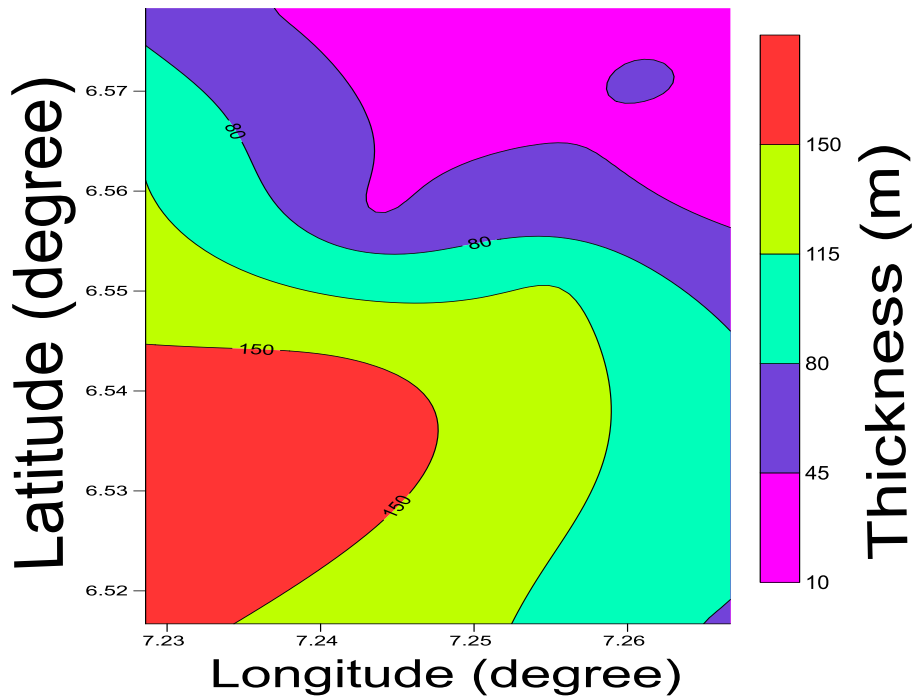


Figure 8b. 2-D contour map showing the distribution of aquifer thickness.

thus be inferred that the aquifers in these regions are sandstone. The study also revealed low values of

protective capacity thus rendering the aquifers vulnerable to contamination. The transmissivity values show high

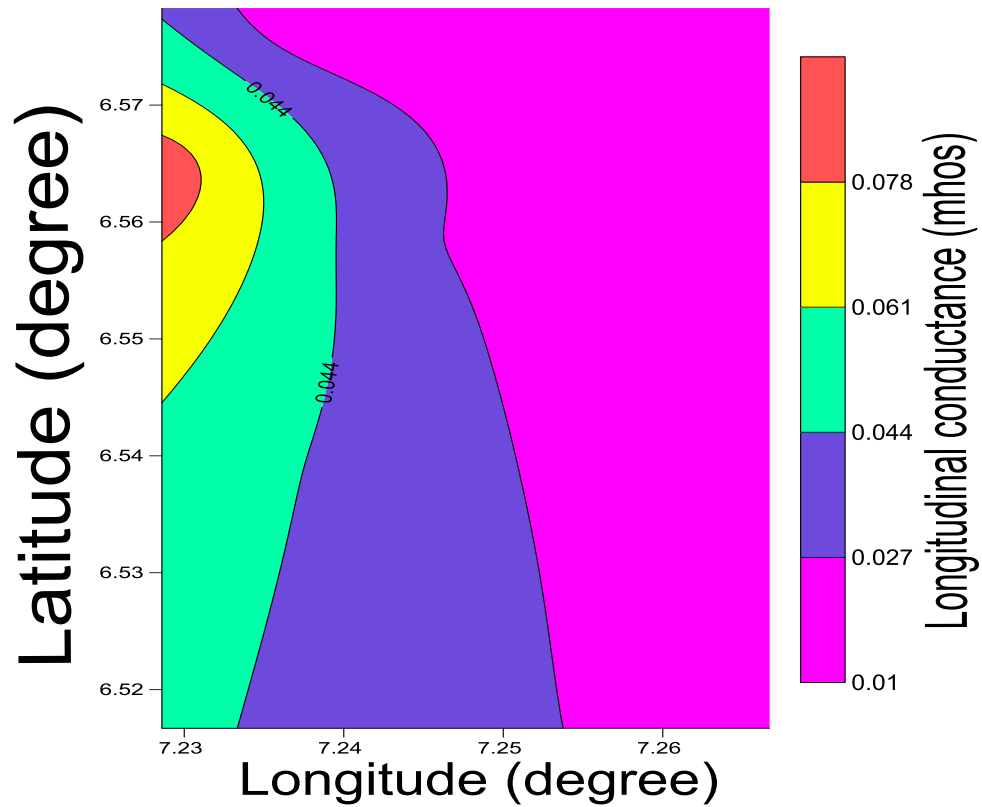


Figure 9. Contour map showing the variation of longitudinal conductance.

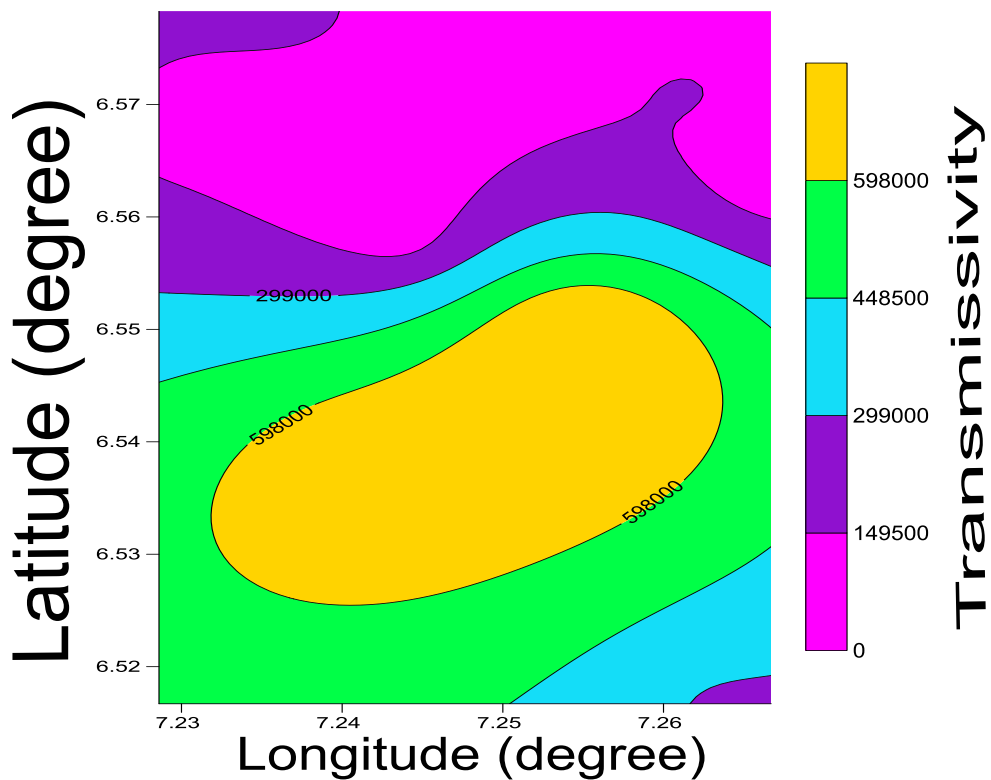


Figure 10. Contour map showing the aquifer transmissivity of the area.

permeability, good groundwater potential and high yield of aquifers that can yield considerable good quantity of water to the inhabitants. This study will serve as a guide to other researchers and borehole drillers for effective groundwater development programmes.

### Conflict of Interest

The authors have not declared any conflict of interest.

### ACKNOWLEDGEMENTS

The authors are grateful to Dr. J. U. Chukudebelu and Dr. P. O. Ezema, both of Department of Physics and Astronomy, University of Nigeria, Nsukka, for their useful contributions.

### REFERENCES

- Agagu OK, Fayose EA, Paters SW (1985). Stratigraphy and Sedimentation in the senonian Anambra basin of Eastern Nigeria. *J. Min. Geol.* 2:25-35.
- Bashir IY, Izham MY, Main R (2014). Vertical electrical sounding investigation of aquifer composition and its potential to yield groundwater in some selected Towns in Bida Basin of North Central Nigeria. *J. Geography Geol.* 6(1):2014.
- Ezeh CE, Ugwu GZ (2010). Geoelectrical Sounding for estimating groundwater potential in Nsukka Local Government Area, Enugu state, Nigeria. *Int. J. Phys. Sci.* 5(5):415-420.
- Ezeh CE, Ugwu GZ, Austin O, Okampa J (2013). Using the relationships between geoelectric and hydrogeological parameters to assess aquifer productivity in Udi Local Government Area, Enugu state, Nigeria. *Int. Res. J. Geol. Mining.* 3(1):9-18.
- Ezeigbo HI, Ozioko DC (1987). Towards efficient rural-water supply to Nsukka area and environs. *Proc., 2nd NISWASA-Symposium Lagos.*
- George N, Obianwu V, Udofia K (2011). Estimation of Aquifer Hydraulic Parameters via Complimenting Surficial Geophysical Measurement by Laboratory Measurements on the Aquifer Core Samples. *Int. Rev. Phys.* 5(2):88-96.
- Hubbard SS, Rubin Y (2005). Introduction to hydrogeophysics. In: *Hydrogeophysics*, eds: Rubin Y, Hubbard SS. Water Science and Technology Library, Springer. The Netherland 50:3-21.
- Ibuot JC, Akpabio GT, George NJ (2013). A survey of repository of groundwater potential and distribution using geoelectrical resistivity method in Itu L.G.A., Akwa Ibom State, Southern Nigeria. *Central European J. Geosci.* 5(4):538-547.
- Lashkaripour GR (2003). An investigation of groundwater condition by geoelectrical resistivity method: A case study in Krin aquifer Southeast Iran. *J. Spatial Hydrol.* 3:1-5.
- Maillet RE (1947). The fundamental equations of electrical prospecting. *Geophysics.* 12:529-556.
- Mamah LI, Ekine AS (1989). Electrical resistivity anisotropy and Tectonism in basal Nsukka formation. *J. Min. Geol.* 25:121-129.
- Mbonu PDC, Ebeniro JO, Ofoegbu CO, Ekine AS (1991). Geoelectric sounding for the determination of aquifer characteristics in parts of the Umuahia Area of Nigeria. *Geophysics* 56(2):284-291.
- McDonald AM, Kemp SJ, Davies J (2005). Transmissivity variations in mudstones. *Groundwater* 43:259-269.
- Niwas S, Singhal DC (1981). Aquifer transmissivity of porous media from Dar-Zarrouk parameters in porous media. *J. Hydrol.* 50:393-399.
- Ofofata GEK (1967). Landforms on the Nsukka Plateau of Eastern Nigeria. *Nig. Geol.* 1(10):3-9.
- Okolie EC (2013). Stratigraphic mapping of subsurface structures and groundwater potentials from electrical resistivity soundings in Onicha Olona, Atumaa Iga and Akwukwu-Igbo, Delta State Nigeria. *Int. J. Water Resour. Environ. Eng.* 5(5):280-288.
- Okpara AI, Onu NN, Okerefor DU (2012). Geophysical sounding for the determination of aquifer hydraulic characteristics from Dar-Zarrouk parameters: case study of Ngor Okpala, Imo River Basin, southeastern Nigeria. *Pacific J. Sci. Technol.* 13:590-603.
- Onugba A, Yaya OO (2008). Sustainable groundwater development in Nigeria. In: *Applied groundwater studies in Africa*, eds. Adelana SMA and MacDonald AM. International Association of Hydrogeologist, CRC Press pp. 103-113.
- Plummer CC (2000). *Physical Geology*, 8th edition. McGraw-Hill Inc., New York.
- Todd DK (2004). *Groundwater Hydrology*, 2<sup>nd</sup> Edition. John Wiley and Sons, New York.
- Utom Au, Odoh BI, Okoro AU (2012). Estimation of Aquifer Transmissivity using Dar-Zarrouk parameters derived from surface resistivity measurements: A case history from parts of Enugu Town (Nigeria). *J. Water Resour. Protection* 4:993-1000.



*Full Length Research Paper*

## Electrical conductivity and uniaxial shear tests on soil samples

Tekin Yeken

Department of Technical Programs, İ. Uzunyol Vocational School, Kocaeli University, TR41800 Hereke/Kocaeli, Turkey.

Received 22 March, 2015; Accepted 13 July, 2015

Soil properties should be well known for the earthquake-resistant structural design studies and other engineering researches. It is aimed to understand the region's soil-structure properties as a result of the practices carried out to determine the mechanical properties and elastic-dynamic character of the units under load. Accordingly, considering the factors that affect the physical and mechanical properties such as mineralogical and petrographic structures, water content, porosity-permeability, chemical composition, texture, and clay-mineral content of the rocks play an important role. Therefore, the data regarding the load-bearing capacity of the ground, seismicity and active tectonics are required for analyzing the study area. In this study, mechanical loading-shear and electrical-resistivity tests were applied simultaneously to the soil samples taken from a seismo-active area in Kocaeli to determine the relationship between these properties. Determination of the electrical resistivity response during the deformation of the material constituted the purpose of this experimental study. Elastic-dynamic parameters were investigated using the relative relationships in terms of physical and mechanical parameters in order to understand the behavior of the sample. The result of experimental study indicated that current increased linearly with the stress before deformation. Similar relationships have been observed for the self-potential parameters and stress. In experiments; sample rate is defined as the axial length of the 1.5 to 2.0% contraction critical threshold. This proportional relationship can be considered in earthquake prediction observation.

**Key words:** Soil investigation, electrical resistivity, potential difference, uniaxial stress, conductivity, deformation.

### INTRODUCTION

Depending on the developing geological technology, several geotechnical applications and laboratory studies have been carried out in order to obtain detailed information on the loading and mechanics of soil (Brace and Orange, 1968; Jaeger and Cook, 1969; Roylance, 2001; Bieniawski, 1992; Bieniawski and Denkhaus, 1994). In such studies, it was aimed to determine the

behaviors of the units constituting the soil under loading as well as the physical and mechanical properties of them. To this end, determination of the elastic-dynamic parameters of the soil is important in terms of the structure-soil relationship.

It is known that rocks under stress are deformed depending on the dynamic properties of the ground and

E-mail: [tyeken@yahoo.com](mailto:tyeken@yahoo.com)

Author(s) agree that this article remain permanently open access under the terms of the [Creative Commons Attribution License 4.0 International License](https://creativecommons.org/licenses/by/4.0/)

its active tectonic effect. As a result of this stress, significant changes occur in the electro-chemical activities and other physical properties of rocks (Brace, 1971; Wawersik and Brace, 1971; Shon, 1998; Clint, 1999). The conductivity of the layers in the ground is determined with the particles forming the layer and the electrical current conductivity capacity of the solution between these particles. Especially, the salinity in the solution and the ambient temperature affect conductivity (Starfield and Fairhurst, 1968; Nasuf, 1977; Idziak and Stan-Kleczeck, 2006). The size of the particles forming the units, the clay content, porosity-permeability and other physical properties of them as well as their loading under pressure are also factors affecting electrical conductivity.

Noticeable changes are observed in the resistivity and potential difference values of the units before and after brittle fracture. Changes which occur in the electromagnetic and other geochemical parameters in a soil layer can be observed periodically. In the study of Brace and Orange (1968), considered one of the first experimental studies on the issue, the electrical resistivities of water-saturated crystalline rocks under the effect of pressure were experimentally correlated. On the other hand, Brace (1971) examined the electrical resistivities of the rock samples during the fracture. Kate and Gokhale (1998) and Kate and Rao (1989) determined the electrical conductivity behaviors of sandstones subjected to uniaxial compression. In a similar study, Idziak and Stan-Kleczeck (2006) determined the physico-mechanical properties of volcanic rock samples and functional relationships of their electrical resistivities experientially.

Deformation of the pre-established static equilibrium with the effect of the additional loading transferred to the ground and regeneration of it is in conformity with the power distribution principle of physics. However, any changes in the mechanical properties of the rocks exposed to deformation due to pressure and stress also occur in their physical properties (Main et al., 1990; Clint, 1999; Kahraman and Yeken, 2008). The bonds between the unit size particles and the relative relationships between the tissues vary depending on the loading and dynamics relationships.

Geological units with high density and no fractures or clay content also usually have high electrical conductivities. As a result of the seismic refraction applications, the layers having these properties were determined to have high seismic velocities as well. On the other hand, rocks containing clay to a certain extent give low resistivity response depending on the amount of the clay. With the physical and mechanical tests implemented for the soil samples taken from any region, important data on the soil dynamics and statics are obtained. In this case, their electrical conductivity varies depending on the clay content and porosity. The purpose of this study is to observe the response of the electrical conductivities on uniaxial shear loading of the ground sample.

In this laboratory work, simultaneously with the electrical parameters of mechanical stress effects were examined. The purpose of this study is the measurement of the electrical parameters in response to pre-deformation of the material.

**METHODS**

Compressional-resistance and electrical conductivity tests were simultaneously applied to the cylindrical samples 50 mm in diameter and 100 mm in height (Figure 1a and b). The samples were divided into three equal parts and copper plates were placed between them in order to provide convenience in theoretical calculations. In the apparatus, the center sections were used for potential difference electrodes and the other connections for current electrodes. Disturbed and undisturbed samples were taken from the field and prepared for the application. The samples were subjected to uniaxial loading at different levels. With the deformation and disturbance occurring as a result of the compressional loading, their self-potential (SP) and electrical current-resistivity response were numerically determined (Figure 2).

In case of diametrical deformation ( $\epsilon_d$ ) and axial unit deformation ( $\epsilon_a$ ), the values are read from the data scale and recorded in each load increase.

$l_0$  = Initial length of the sample,  $\Delta l$  = When the change in the length of the sample is taken;

Axial unit deformation ( $\epsilon_a$ ),  $\epsilon_a = \frac{\Delta l}{l_0}$

**Electrical resistivity**

In the general sense, it is defined as the measurement of the potential distribution of the electric field in the ground generated by the electric current transferred into the ground. Determination of the potential value at a distance of ( $l$ ), at a given point in a homogeneous and isotropic medium constitutes the purpose of the resistivity method. A homogeneous medium was chosen in order to ground the method on a more simple and basic mathematical basis. Resistance of a circuit is expressed as follows according to Ohm's law;

$R = \Delta V / \Delta I \quad (\Omega)$

However, the resistance for an element with L dimension and  $V_A$  cross-section is expressed as follows (Figure 3):

$R = \rho L / A$

The following expression is obtained from here;

$\Delta V / \Delta I = \rho \cdot L / A$

$\Delta V = \rho \cdot \Delta I \cdot L / A$

$\Delta V$ : Potential difference (mV),  $\rho$ : Resistivity (Ohm-m),  $\Delta I$ : Current (mA), L: Length (m), A: Cross section ( $m^2$ ), G:Geo. Constant,  
 $-\int dV = \rho I \int dr / ds$   
 $-V = \rho I / 4\pi \int dr / r^2$

Due to the semi-infinite surface, the following expressions are obtained;

$\Delta V = \rho \cdot I / 2\pi 1 / r$

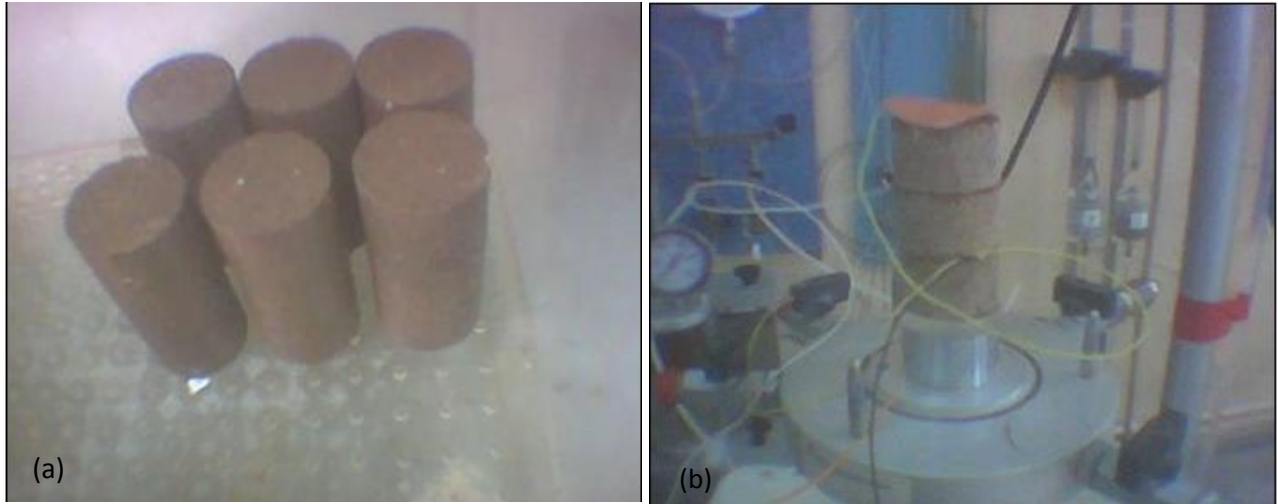


Figure 1. (a) Soil sample, (b) Uniaxial shear test and electrical measurement apparatus.

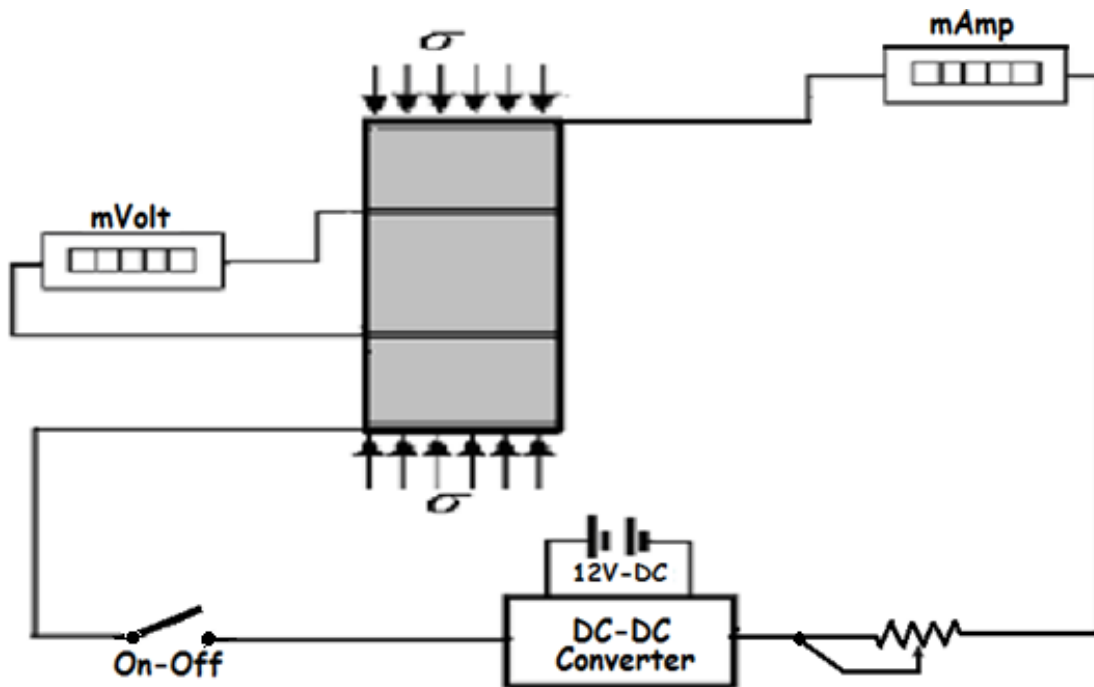


Figure 2. Mechanical and electrical test diagram.

Resistivity from generalized equation;

$$\rho = G \cdot (\Delta V / I) \text{ (}\Omega\text{m)}$$

**Potential difference**

In the implementation, uniaxial stress and its consequential natural potential relationship were measured. It is based on the basis of the potential difference change depending upon the amount of the

pressure. The differences in the physical properties of the samples cause potential difference change. In natural environment, there are secondary potentials which occur as a result of the electrochemical reactions such as vegetation potential arising from bioelectrical activities and diffusion potential caused by liquid flows in the earth. However, galvanic potentials which occurred as a result of the concentration differences between the particles were measured for the samples used in the experiment. Uniaxial shear and resistance tests were applied to the samples and potential difference changes of the material were examined during the deformation period

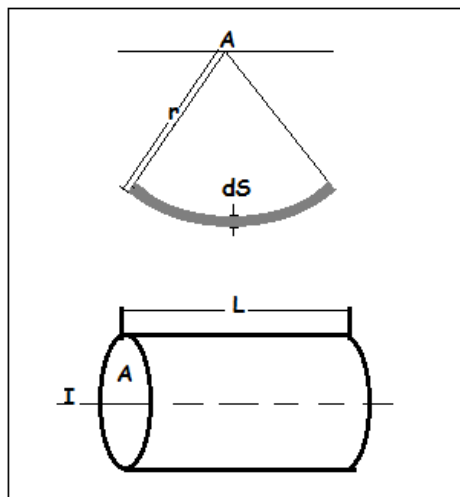


Figure 3. Resistivity of an element with unit size and unit area.

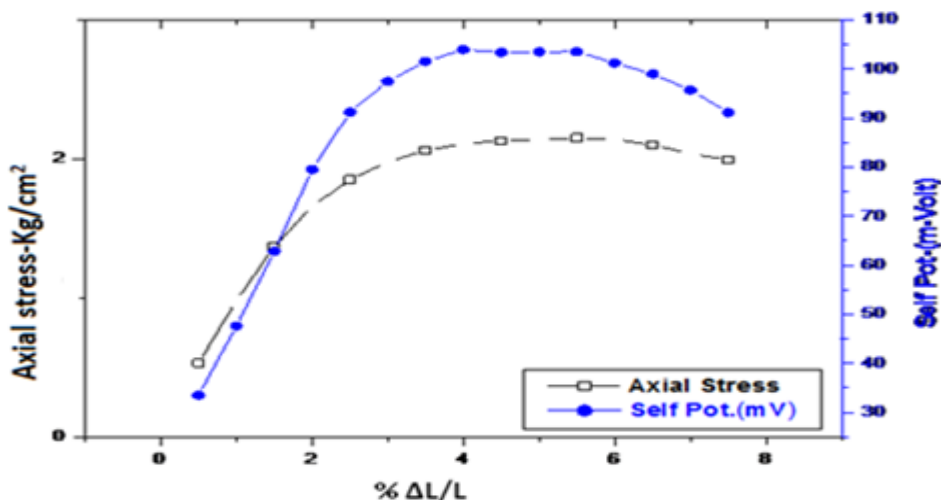


Figure 4. Potential difference changes versus axial stress. (Sample:A-01).

(Figures 4 to 13).

**EVALUATION**

In monitoring the changes in the electrical and mechanic parameters in these studies, petro-physical property of the environment is taken into consideration in especially fine-grained soils. In the determination of seismic “gap” areas and risk-bearing regions, the prediction modellings to be applied are important. In especially prediction modelling studies, the self-potential values and resistivity relationship of the fine-grained clayey-silty layer can be monitored more specifically than rock units with high

mechanical endurance. On the other hand, monitoring the parameters for prediction in pre-earthquake period (foreshock) can provide important nonnumeric cues about critical anomaly and energy discharge as a result of brittle fracture.

In the study, the soil samples analyzed under uniaxial stress were examined in disturbed and undisturbed forms. Electrical resistivity and current-potential difference behaviors of the disturbed samples under axial stress were correlated (Figures 4 to 13). In Figures 4, 5 and 6; potential difference responses depending on the applied axial stress were determined. A curvilinear cohesion is observed until the material deformation limit. However, SP values tend to decrease sharply with the

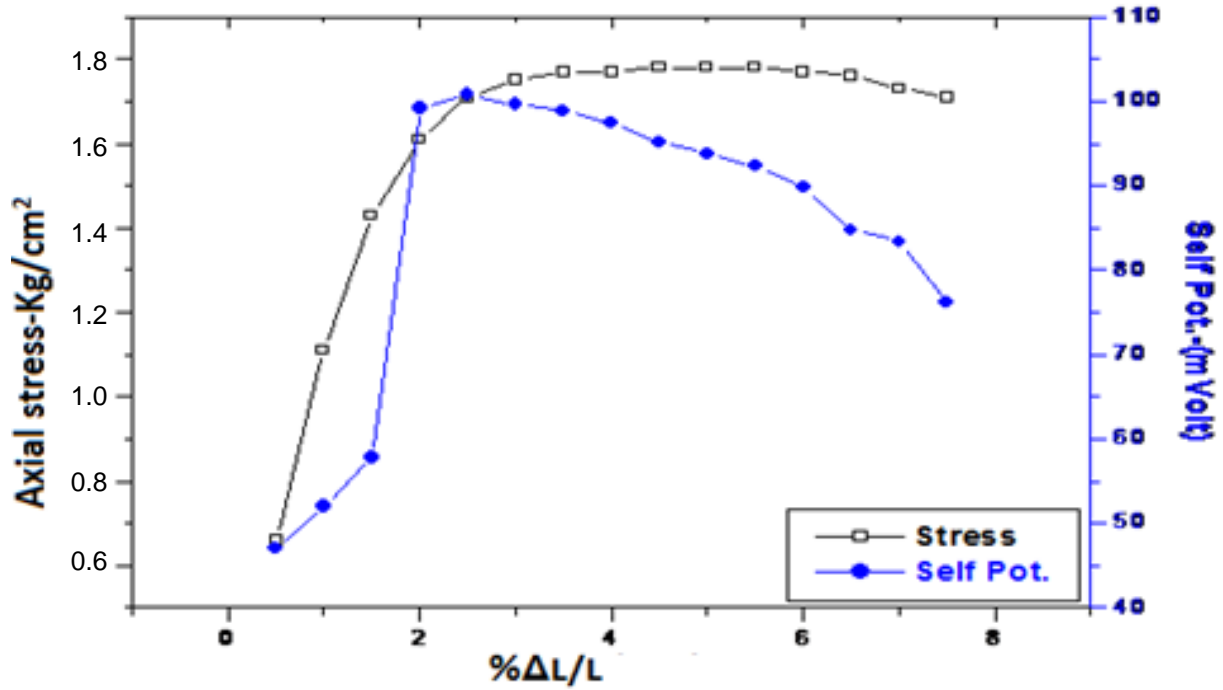


Figure 5. Potential difference changes due to the axial stress. (Sample:A-02).

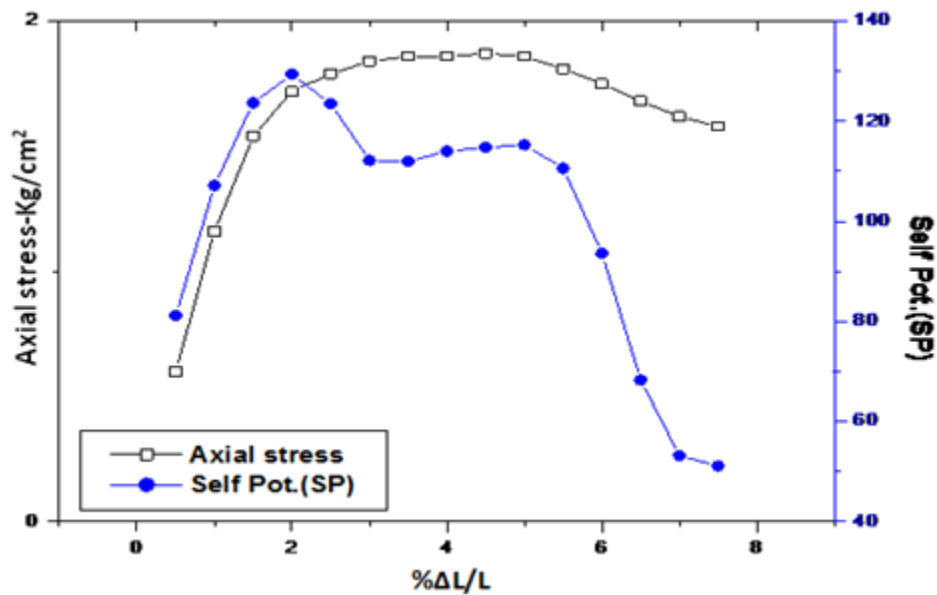


Figure 6. Potential difference changes due to the axial stress. (Sample:A-03).

increase in the fractured medium as a result of the loading dependent on the swelling of the material. In Figure 7, the relationship between the axial stress and resistivity was analyzed. As the elastic material was compressed with pressure, the electrical resistivity values decreased in an inverse proportion. In Figures 8 and 9,

the change in the current given to the circuit under compressive stress was specified. For both samples, post-deformation current behaviors are compatible. In Figure 10, the functional relationship between the current given to the material and the inversely proportional change in the potential difference is compatible according

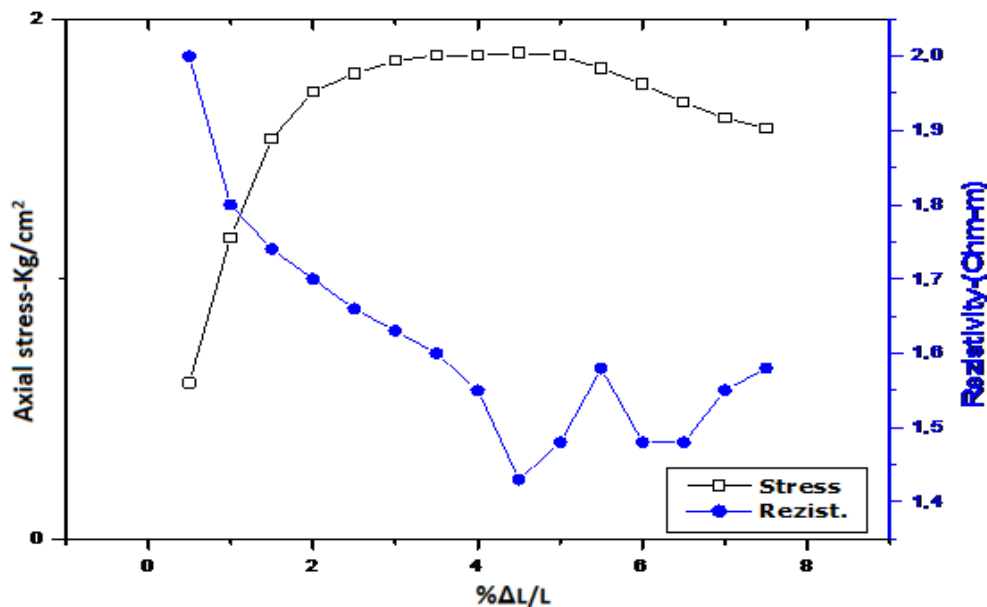


Figure 7. Resistivity versus axial stress (Sample:A-04).

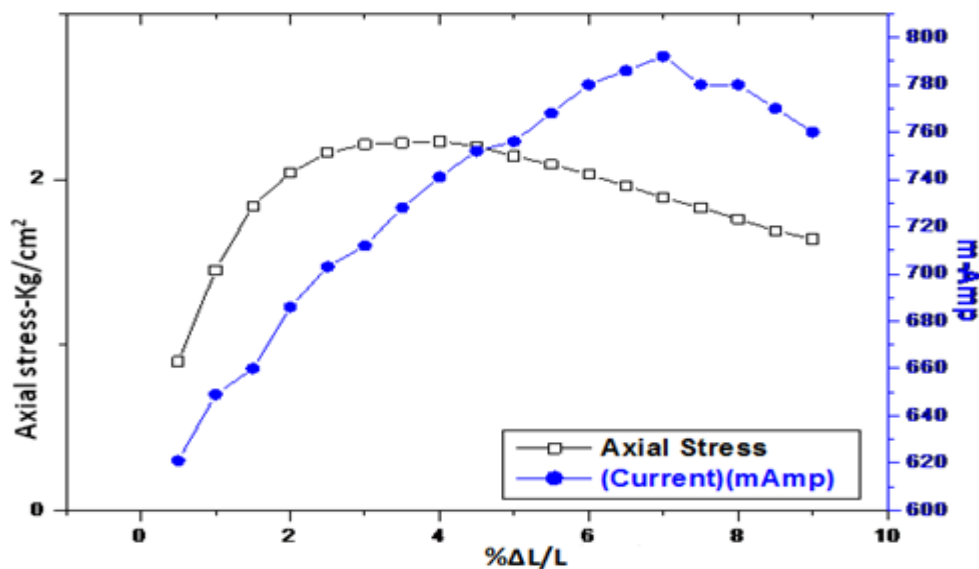


Figure 8. Current versus axial stress (Sample:A-05).

to the Ohm principle and theory. In Figures 11 and 12, the SP relationships of the undisturbed samples (UD) under axial stress were determined. In Figure 13, the current, stress and proportional relationships in case of longitudinal construction (%DL/L) were determined.

**DISCUSSION AND CONCLUSION**

The following findings were obtained according to the

studies carried out:

- (i) Determination of the responses of electrical parameters to be created for the medium with the effect of loading in a soil sample with high activity constituted the purpose of this study.
- (ii) In this experimental study, a uniaxial construction at a rate of approximately 1.5 to 2.0% was observed in the length of the material with a linear loading in fine-grained soils. On the other hand, an increase was observed in the

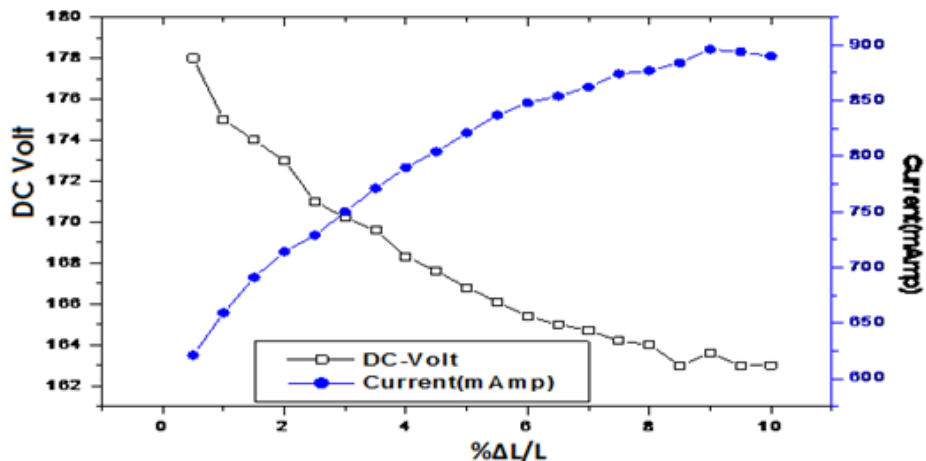


Figure 9. Current versus DC voltage (Sample:A-07).

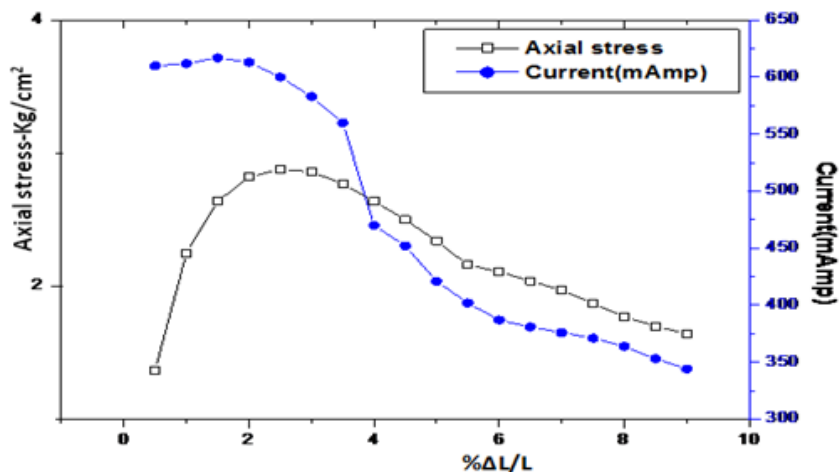


Figure 10. Current versus axial stress (Sample: A-10).

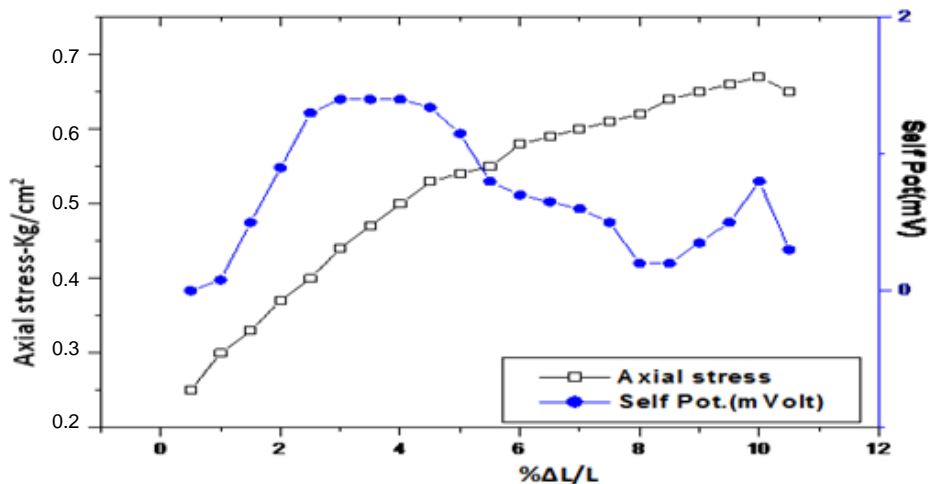


Figure 11. Self potential (SP) versus axial stress (A/UD-13).

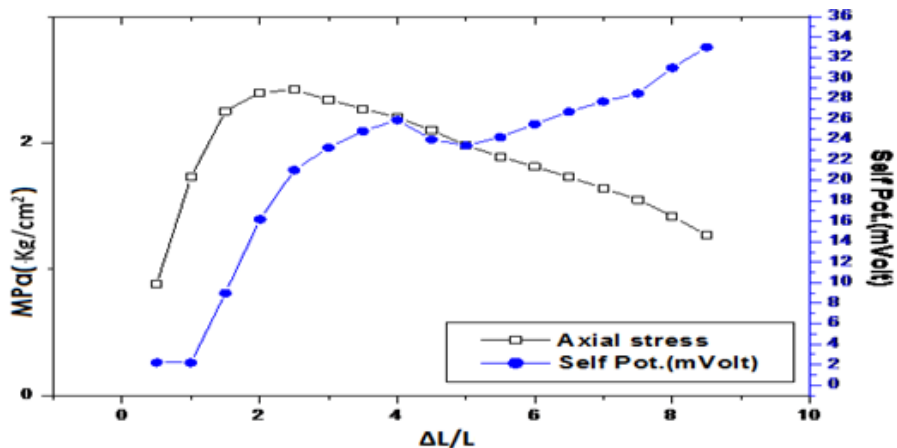


Figure 12. Self Potential (SP) versus axial stress (A-1/UD14).

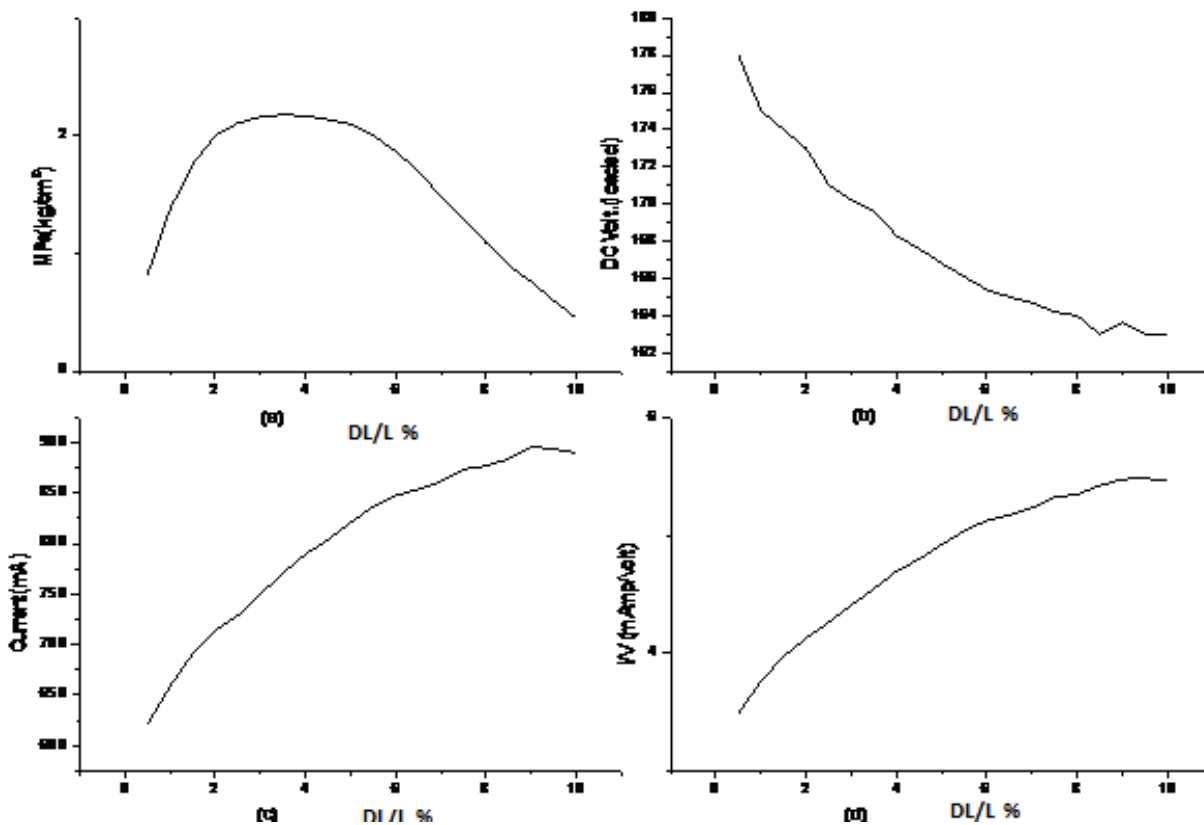


Figure 13. Axial stress, current and potential difference (A-1(07)). (a) Axial stress(Mpa), (b) DC voltage versus the circuit, (c) Current change (mA) versus  $\Delta L/L$  %, (d)  $I(\text{mA}) / \text{mV}$  proportional change.

electrical conductivity until the fracture process of the material, whereas the conductivity values behaved erratically during the ductility or dispersion process of the material.

(iii) In the earthquake prediction studies, the periodic resistivity measurement technique correlated with the

other electrical parameters is quite important. It is known that there will be increases in the resistivity values due to the pre-brittle fracture micro-tensile cavities in a rock under compressional stress. However, in response to the increase in pressure, there is an inversely proportional and sharp decrease in the resistivity values in a fine-



grained compressed soil.

### Conflict of Interest

The authors have not declared any conflict of interest.

### ACKNOWLEDGEMENT

Author would like to thank the General Directorate of State Hydraulic Works (DSİ) – Department of Technical Research and Quality Control (TAKK) (Ankara), Soil Laboratory Branch Office and employees.

### REFERENCES

Brace WF, Orange AS (1968). Electrical resistivity changes in saturated rocks during fracture and frictional sliding: *JGR* 73(4):1433-1445.

Brace WF (1971). Resistivity of saturated crustal rocks to 40 km based on laboratory measurements; GG. Heacock, ed. *The Structure and Physical Properties of the Earth's Crust.*: AGU, Washington, D.C. Geophys. Monog. Ser. P. 14.

Jaeger JC, Cook NGW (1969). *Fundamentals of Rock Mechanics* Methuen, LONDON.

Wawersik WR, Brace WF (1971). Postfailure behaviour of a granite and diabase. *Rock Mech.* 3:61-85.

Bieniawski ZT, Denkhaus HG (1994). Failure of fractured rock. *Int. J. Rock. Mech. Mineci.* 6(3):123-145.

Roylance D (2001). *Introduction to Fracture Mechanics*, Massachusetts Institute of Techn. Cambridge, MA. 02139.

Starfield AM, Fairhurst C (1968). How high-speed computers advance design of practical mine pillar system. *Eng. Mining J.* P.169.

Bieniawski ZT (1992). *Design Methodology in Rock Engineering.* ISBN-13:978-9054101215.

Nasuf SE (1977). A photo-elastic and Field investigation into the Interface problem in Rock Mechanics, Rhd thesis Univ. Strathclyde.

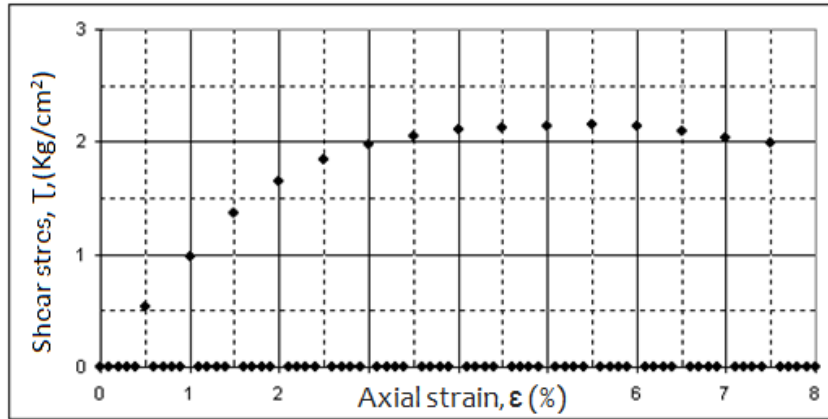
Idziak AF, Stan-Kleczyk I (2006). Predicting the physico-mechanical properties of igneous rocks from electrical resistivity measurements, EUROCK 2006-Multiphysics Coupling and Long Term Behavior in Rock Mechanics, ISBN 0415410010, London.

Shon JH (1998). *Physical properties of rocks: Fundamentals and principles of petrophysics*, Elsevier, Oxford. L P. 582.

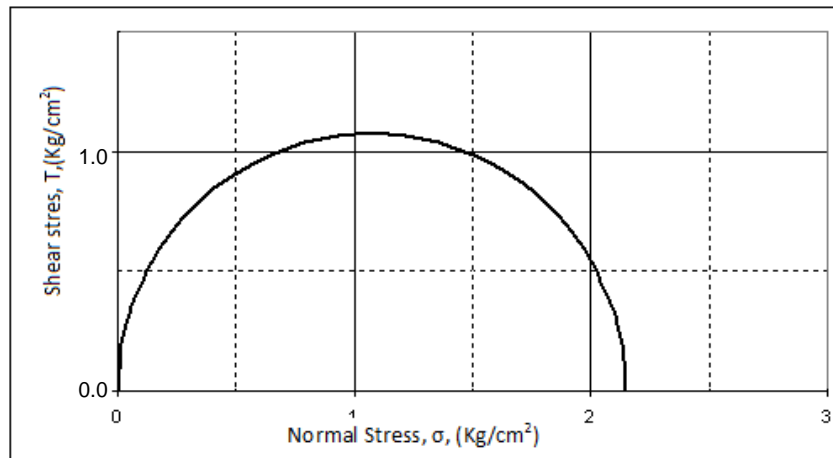
Main IG, Meredith PG, Sammonds PR, Jones C (1990). Influence of fractal flaw distributions on rock deformation in the brittle field. In *Deformation Mechanisms, Rheology and Tectonics*, Knipe RJ, and Rutter EH, *Geol. Soc. Lond. Special Publication.* 54:81-96.

Kahraman S, Yeken T (2008). Determination of physical properties of carbonate rocks from P-wave velocity. *Bull. Eng. Geol. Env.* 67:277-281.

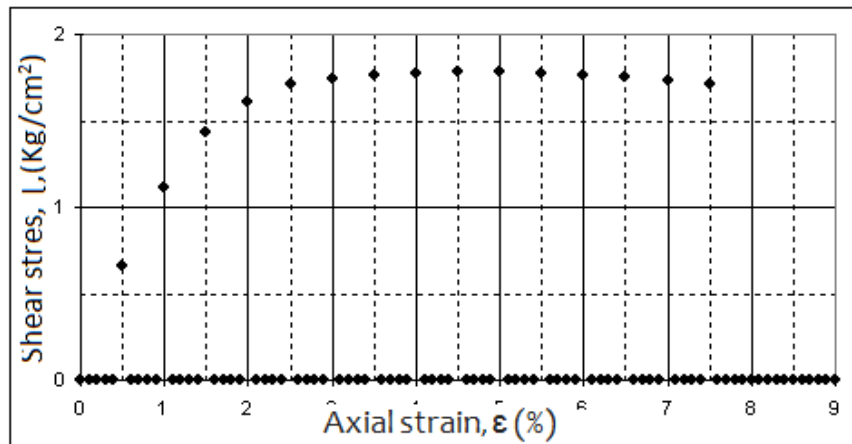
APPENDIX



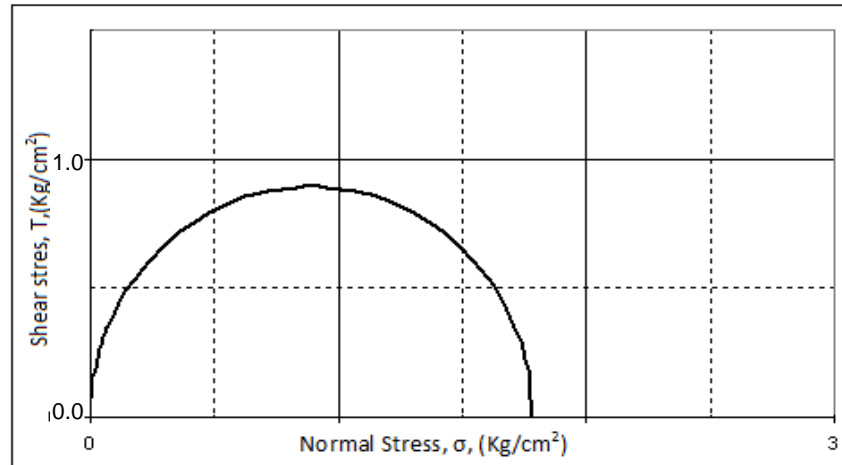
Sample no:A-1(01):  $q_u$  (kg/cm<sup>2</sup>):2,15  $\Delta L/L$  (%):5,50.



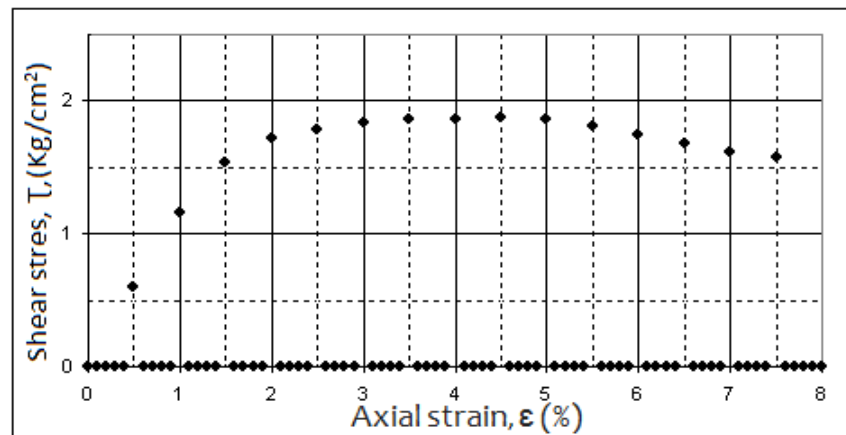
A (cm<sup>2</sup>): 20,778 F(kg):44,6.



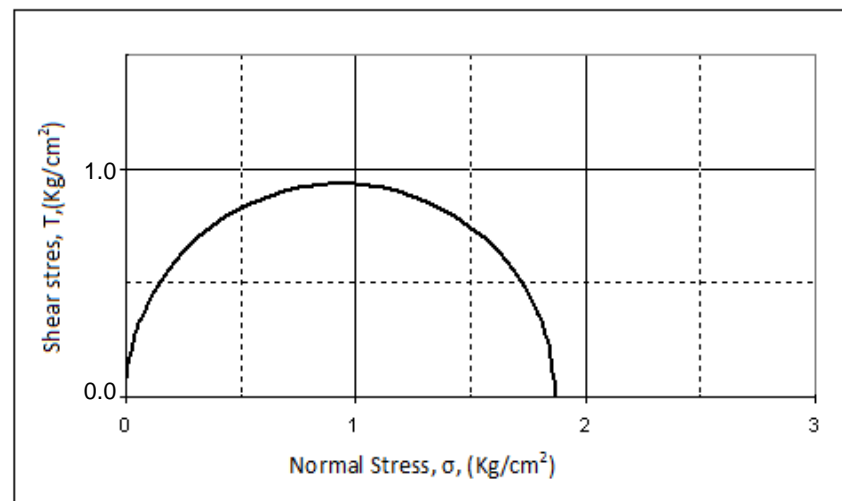
Sample no:A-1(02):  $q_u$  (kg/cm<sup>2</sup>):1,78  $\Delta L/L$  (%):5,00.



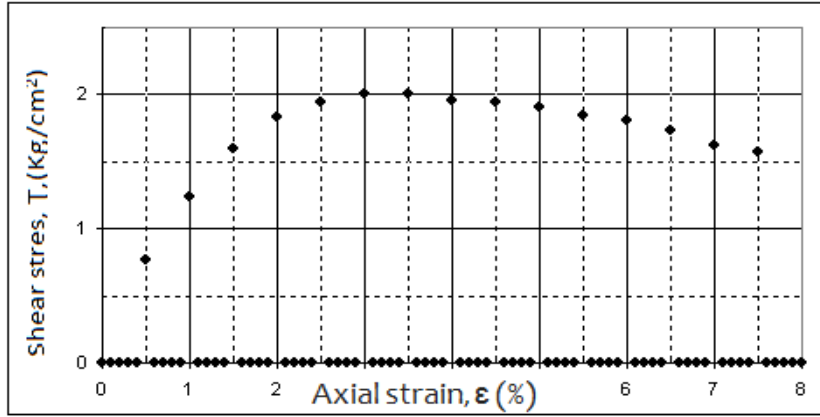
$A$  ( $\text{cm}^2$ ): 20,668  $F$  (kg): 36,9.



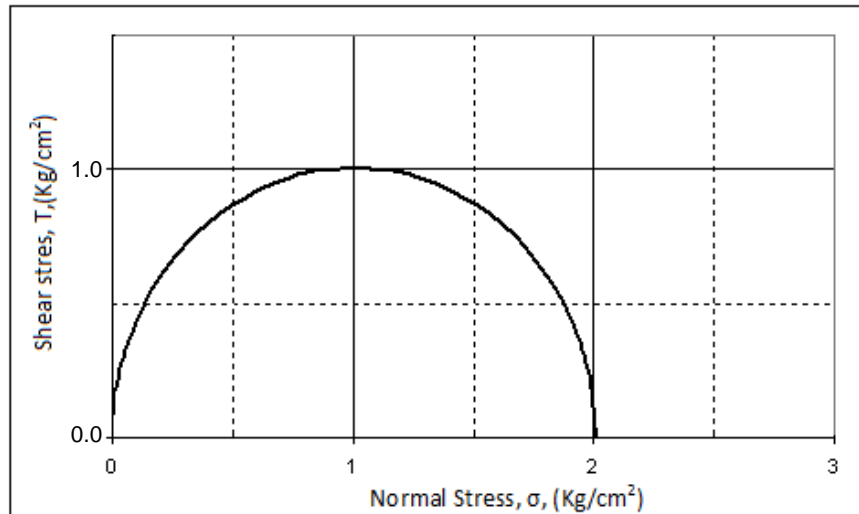
Sample no:A-1(03):  $q_u$  ( $\text{kg}/\text{cm}^2$ ):1,87  $\Delta L/L$  (%):4,50.



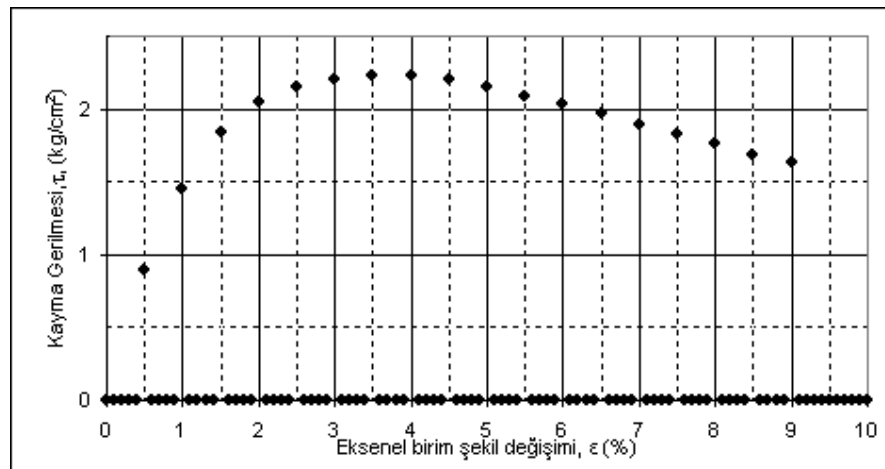
$A$  ( $\text{cm}^2$ ): 20,560  $F$  (kg): 38,4.



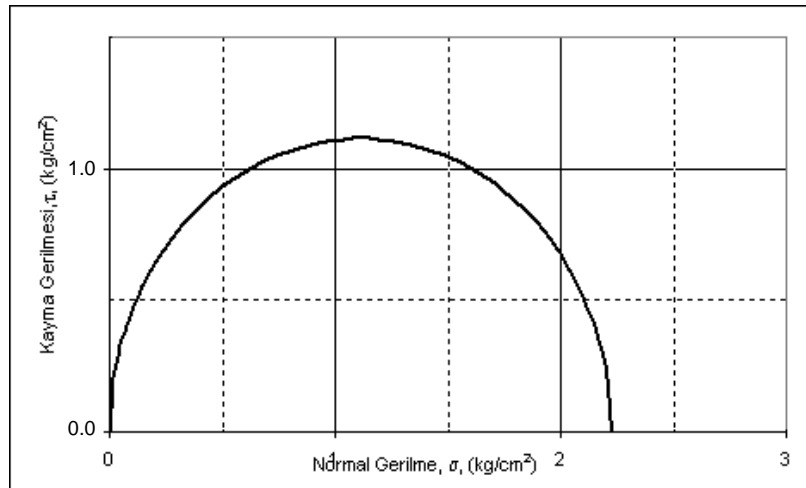
Sample no:A-1(04):  $q_u$  (kg/cm<sup>2</sup>):2,01  $\Delta L/L$  (%):3,50.



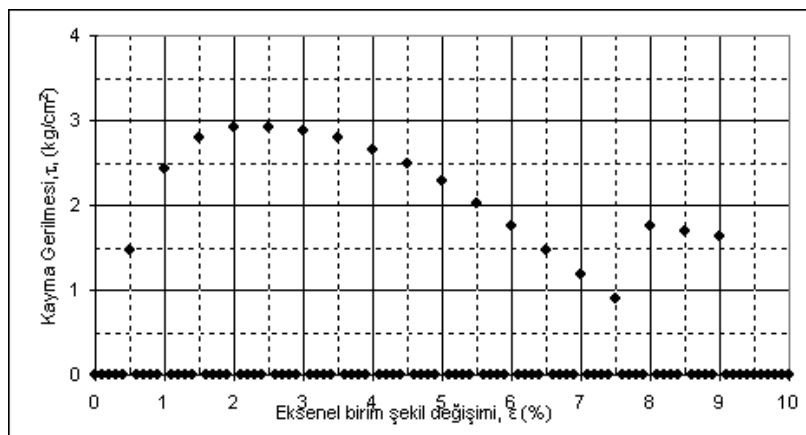
A (cm<sup>2</sup>): 20,347 F (kg): 40,9.



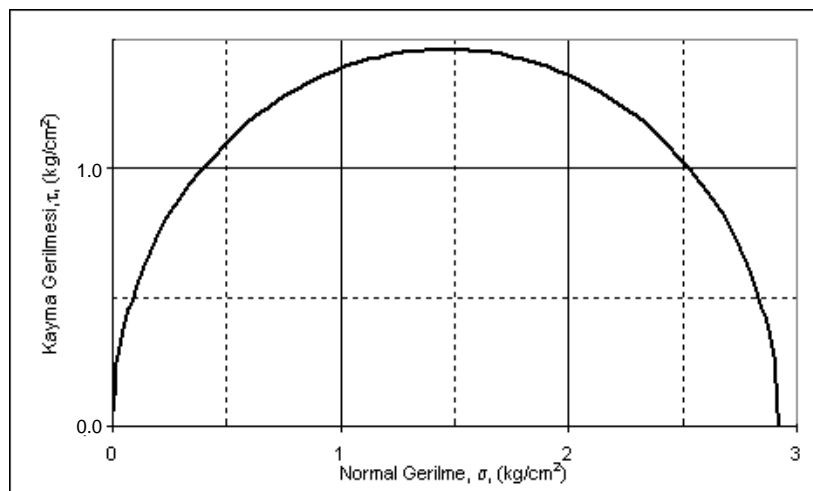
Sample no:A-1(05):  $q_u$  (kg/cm<sup>2</sup>):2,23  $\Delta L/L$  (%):4,00.



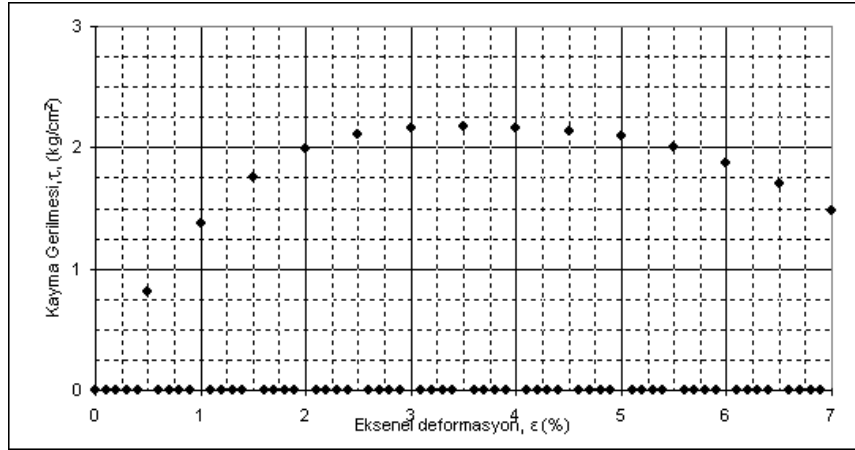
**A** (cm<sup>2</sup>): 20,453 **F** (kg): 45,6.



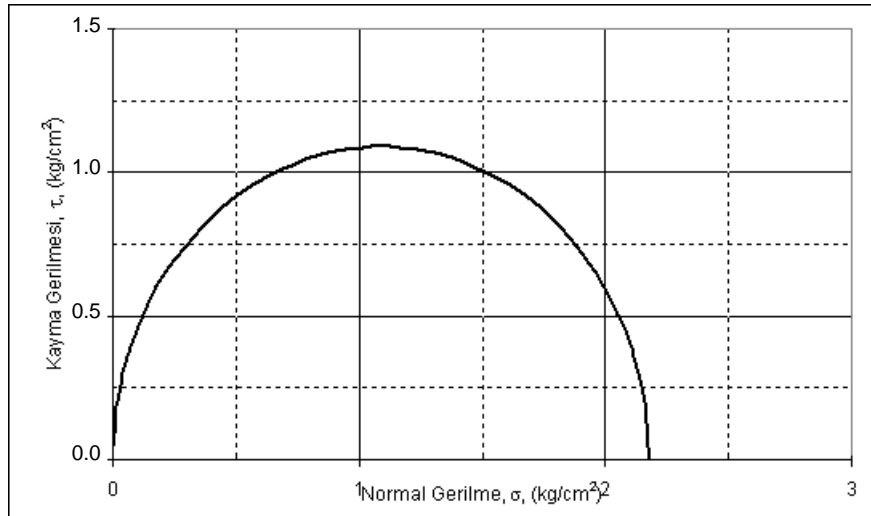
**Sample no:**A-1(06): **q<sub>u</sub>** (kg/cm<sup>2</sup>):2,92 **ΔL/L**(%):2,0.



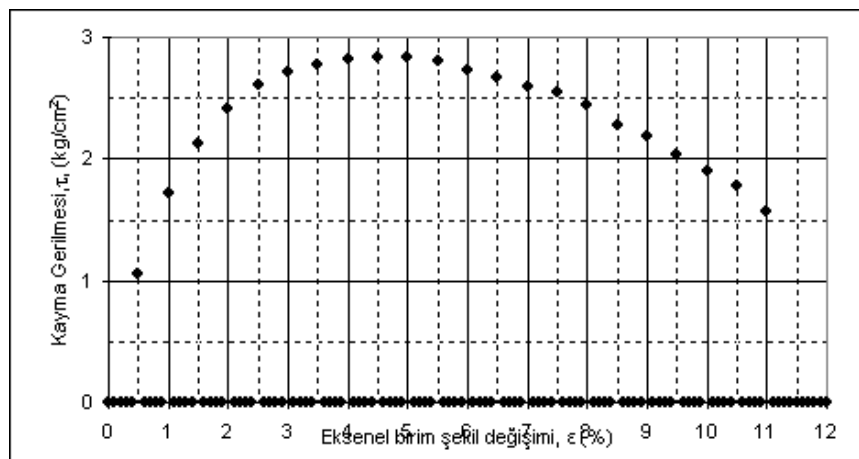
**A** (cm<sup>2</sup>): 20,036 **F** (kg): 58,6.



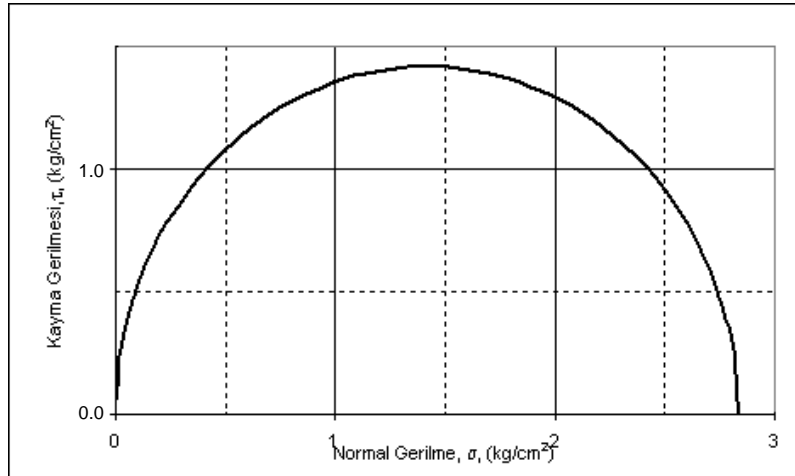
Sample no:A-1(07):  $q_u$  (kg/cm<sup>2</sup>):2,18  $\Delta L/L$ (%):3,5.



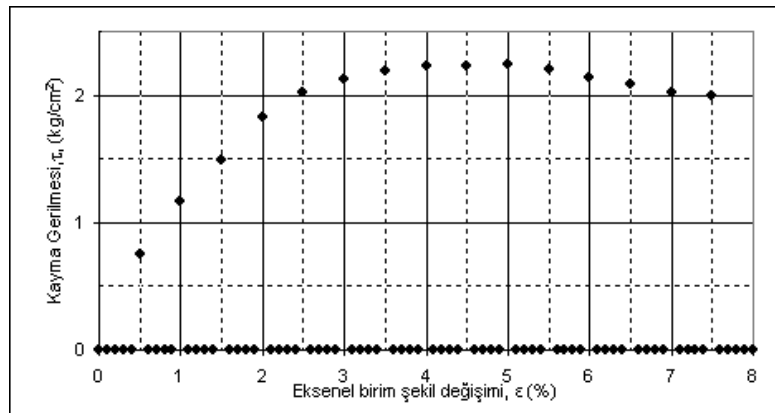
A (cm<sup>2</sup>): 20,347 F (kg): 44,3.



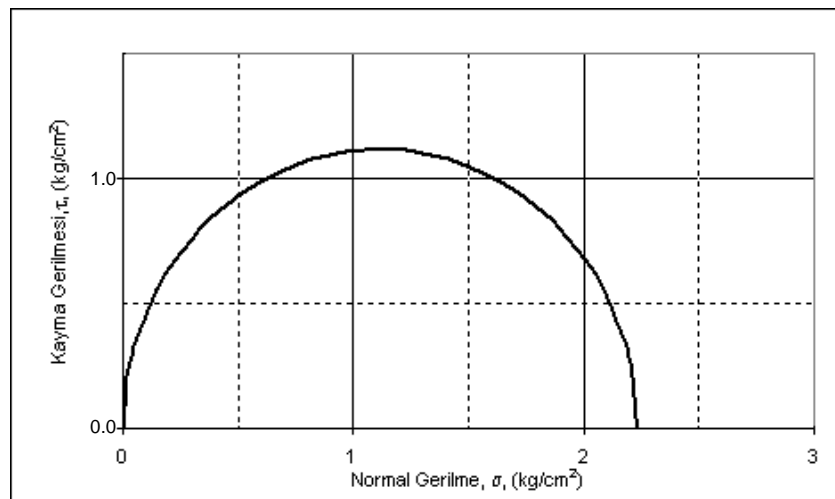
Sample no:A-1(08):  $q_u$  (kg/cm<sup>2</sup>):2,83  $\Delta L/L$ (%):5,0.



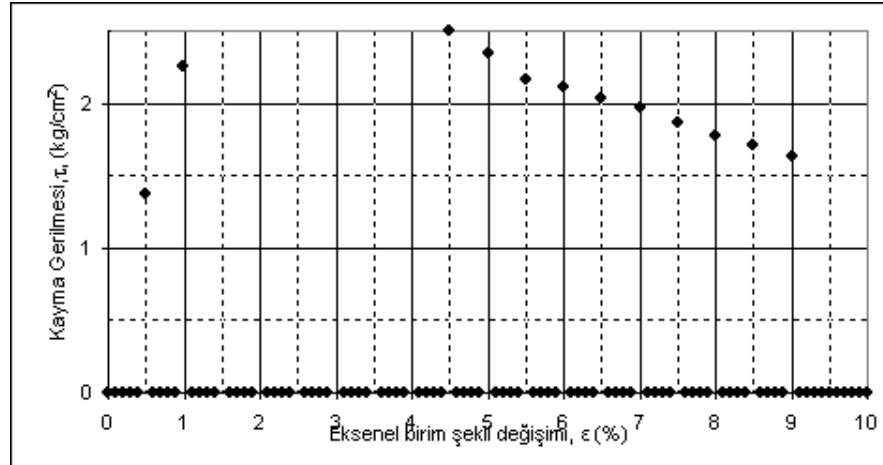
A (cm<sup>2</sup>): 20,668 F (kg): 56,8.



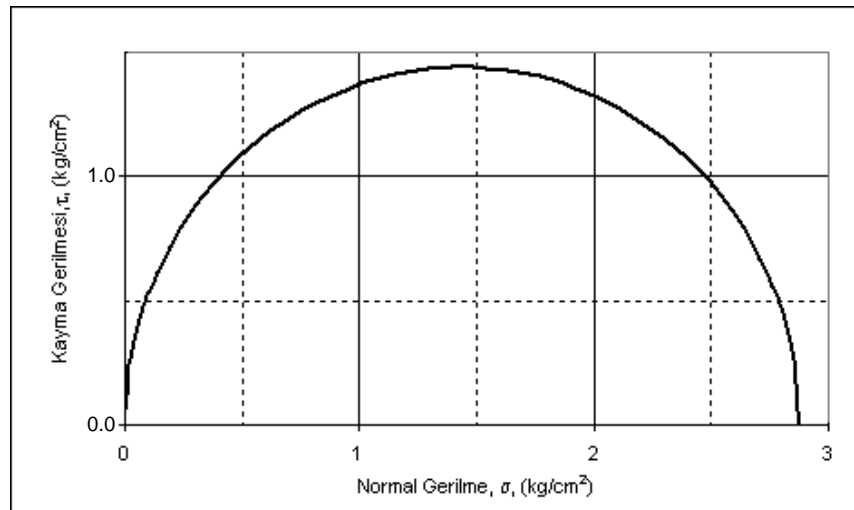
Sample no:A-1(09):  $q_u$  (kg/cm<sup>2</sup>):2,23  $\Delta L/L$ (%):5,0.



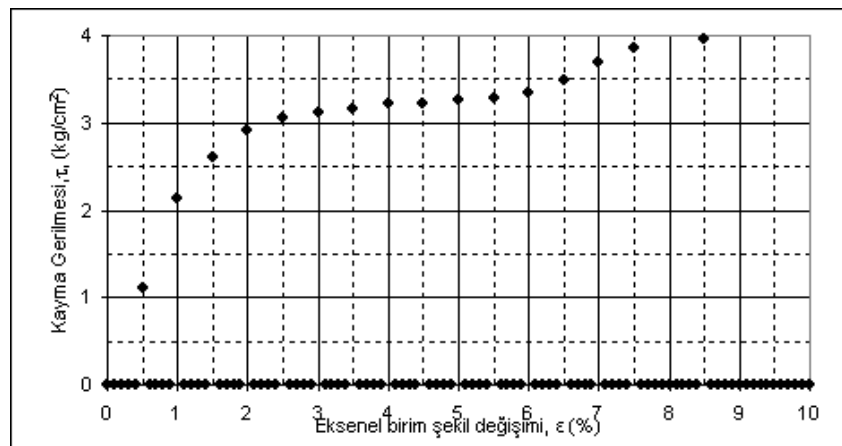
A (cm<sup>2</sup>): 20,668 F (kg): 46,2.



Sample no:A-1(10):  $q_u$  ( $\text{kg/cm}^2$ ):2,88  $\Delta L/L$ (%):2,5.

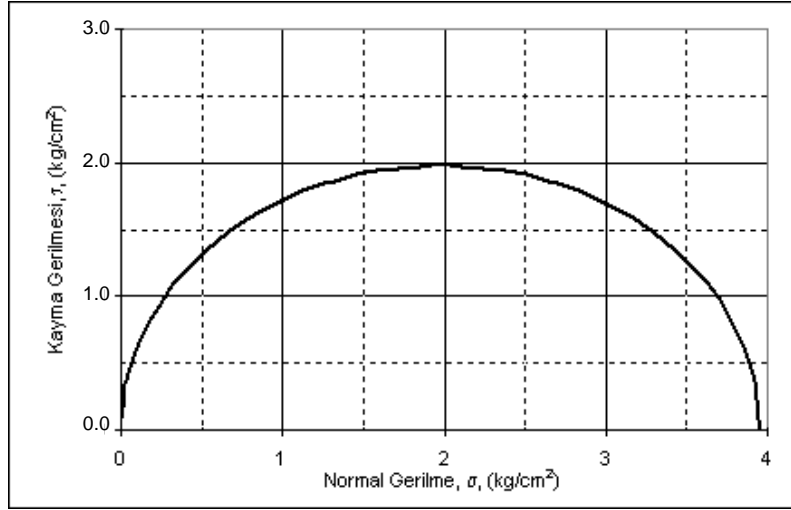


A ( $\text{cm}^2$ ): 20,138 F (kg): 58,0.

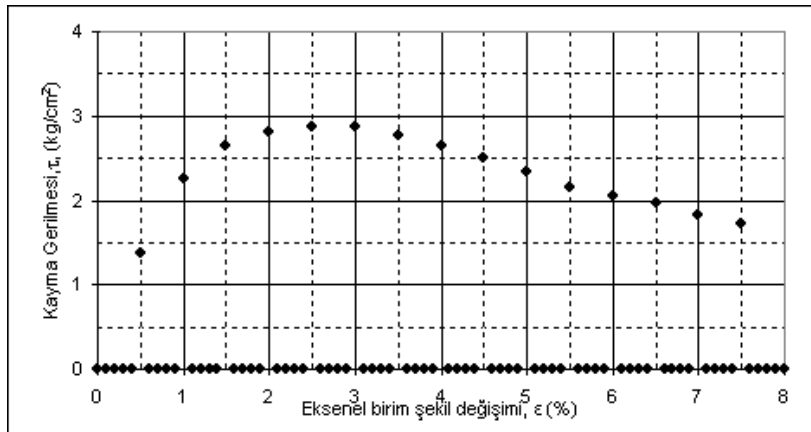


Sample no:A-1(11):  $q_u$  ( $\text{kg/cm}^2$ ):3,96  $\Delta L/L$ (%):3,96.

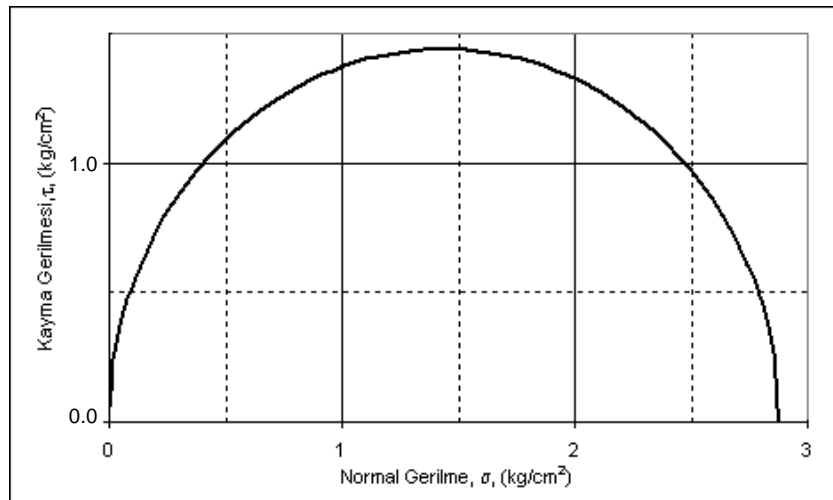




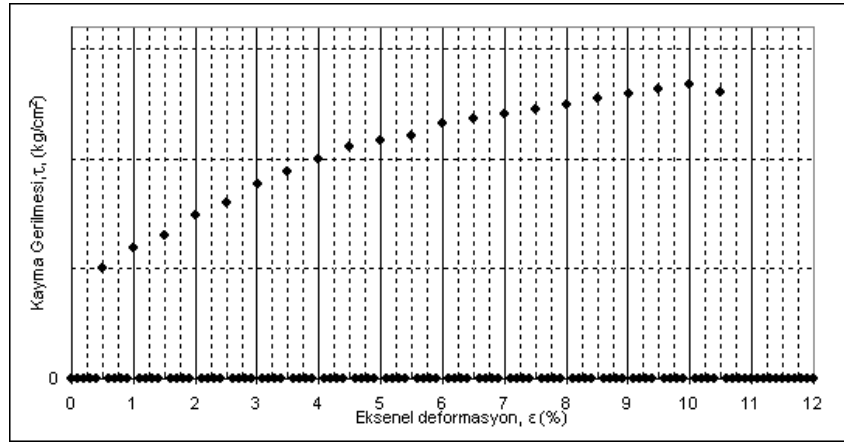
A (cm<sup>2</sup>): 21,459 F (kg):84,9.



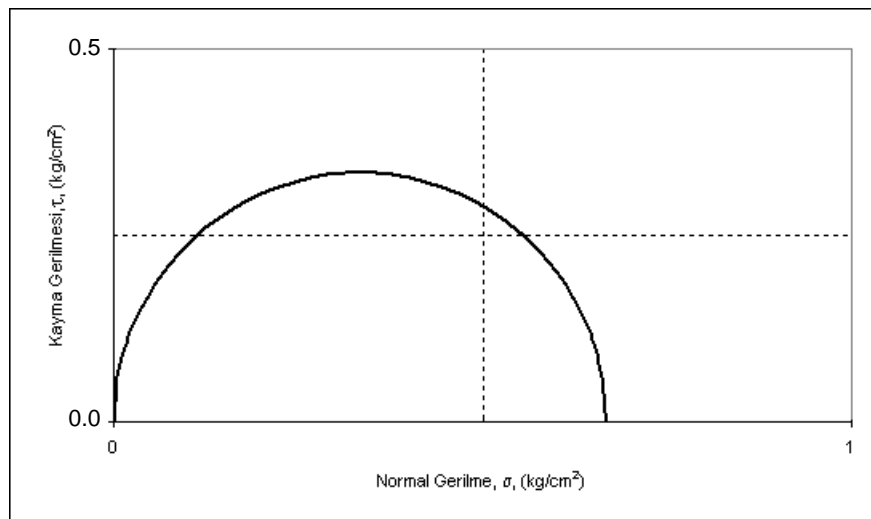
Sample no:A-1(12):  $q_u$  (kg/cm<sup>2</sup>):2,18  $\Delta L/L$ (%):4,9



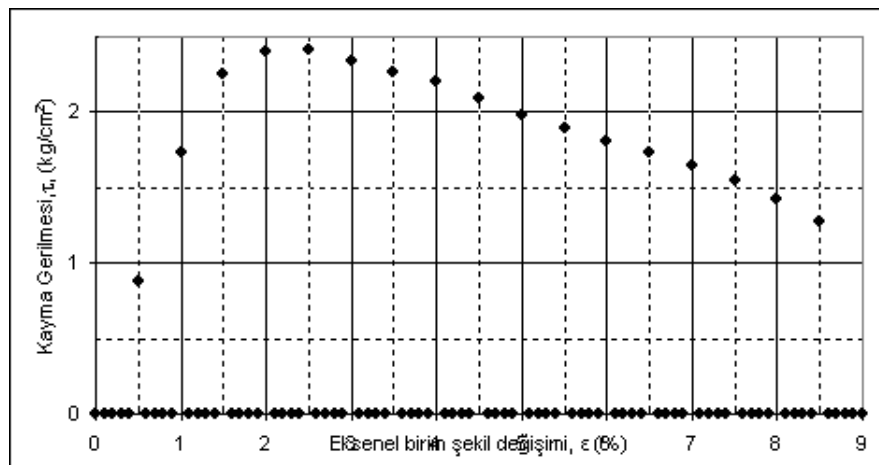
A (cm<sup>2</sup>): 19,48 F (kg): 46,2.



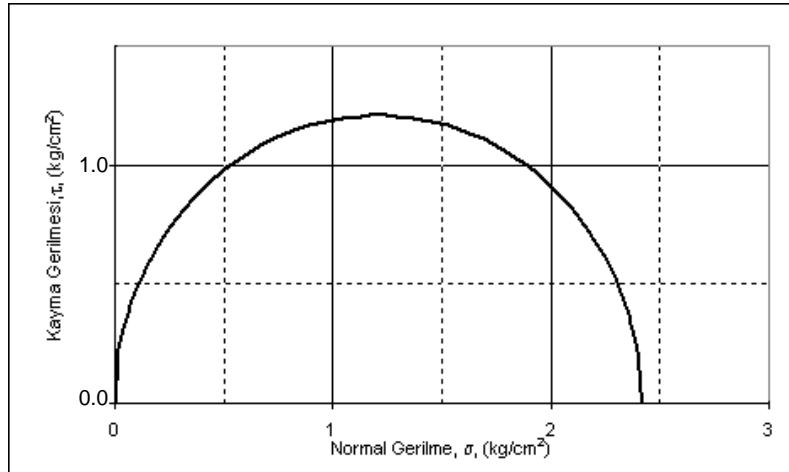
Sample no:A-1(13):  $q_u$  (kg/cm<sup>2</sup>):0,67  $\Delta L/L$ (%):10,0.



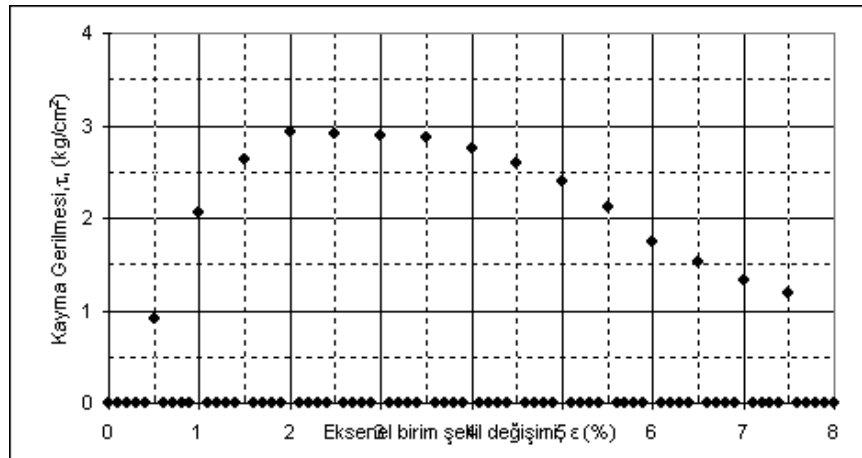
A (cm<sup>2</sup>): 21,817 F (kg): 14,6.



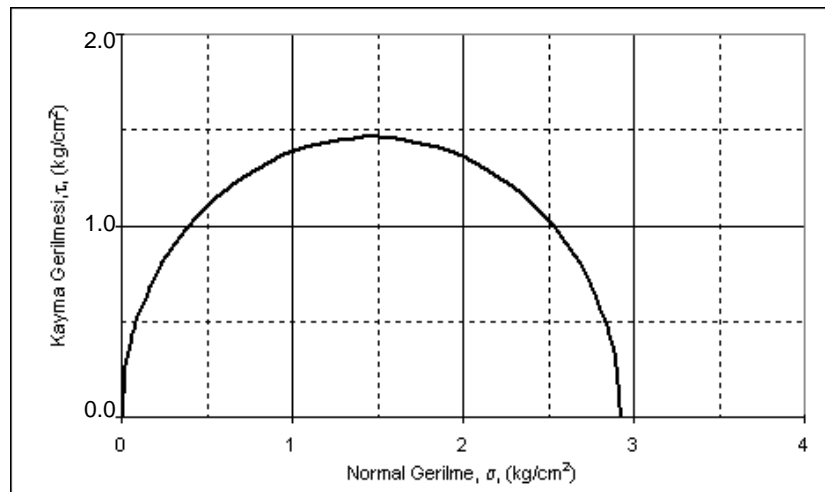
Sample no:A-1(14):  $q_u$  (kg/cm<sup>2</sup>):2,42  $\Delta L/L$ (%):2,5.



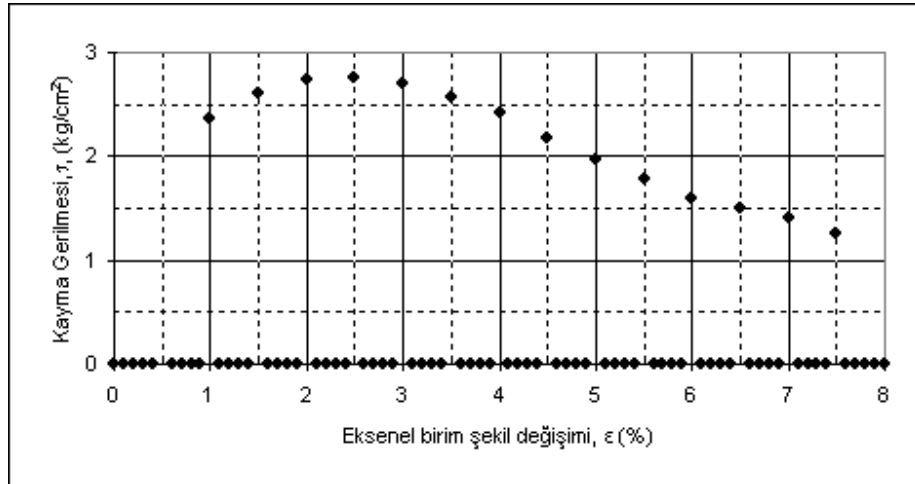
A (cm<sup>2</sup>): 20,138 F (kg): 48,7.



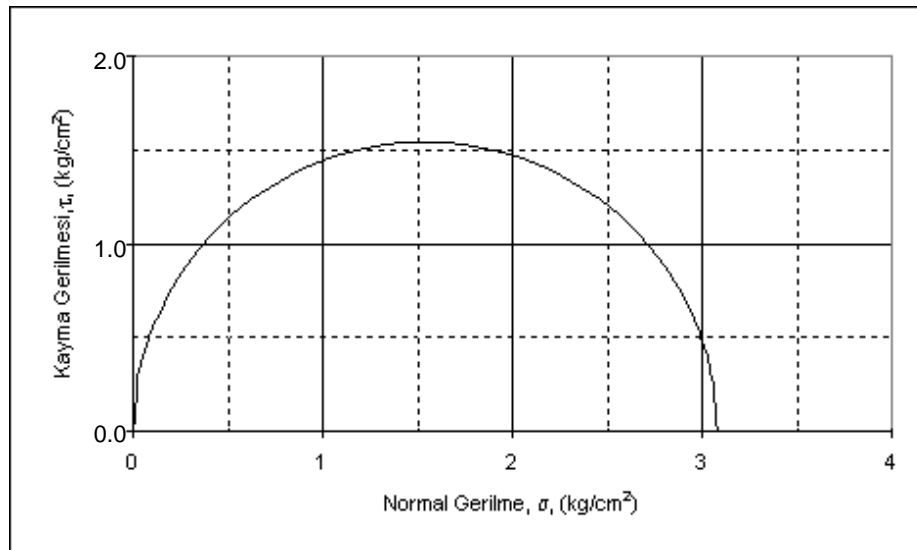
Sample no:A-1(15):  $q_u$  (kg/cm<sup>2</sup>):2,92  $\Delta L/L$ (%):2,0.



A (cm<sup>2</sup>): 20,036 F (kg): 58,6.



Sample no:A-1(16):  $q_u$  (kg/cm<sup>2</sup>):3,09  $\Delta L/L$ (%):0,5.



A (cm<sup>2</sup>): 19,734 F (kg): 60,8.

*Full Length Research Paper*

## General Relativity support from the double pulsar

Keith John Treschman

51 Granville Street Wilston 4051 Australia.

Received 25 June, 2015; Accepted 27 July, 2015

After the final publication of the Theory of General Relativity by Albert Einstein in 1916, experimental confirmation rested on three astronomical tests. These were the amount of bending of starlight at the edge of the Sun, the change in frequency of light emanating from the gravitational field of the Sun and an explanation in terms of the theory of a remnant quantity in the perihelion advance of Mercury which had been calculated previously. The field of activity then was sparse and Quantum Mechanics attracted many scientists to its realm. However, a proliferation of renewed interest emerged 50 years on from 1916 with new thinking, improved instrumentation, the advent of spacecraft and the discovery of a number of exotic objects. The previous tests had been within the solar system. Now, there could be a transition from a weak to strong gravitational field testing. Neutron stars and pulsars were proposed based on ideas inherent within Einstein's conjecture as explanations for otherwise mysterious radio signals. In 2003, the advent of a two pulsars in mutual orbit allowed astrophysicists to delve into more precise tests of Einstein's theory. One of the parameters measured with this double pulsar has agreed with General Relativity to the 0.05% level. Three others are different from predictions by 1.4, 0.68 and 5.5%. Testing of these other parameters over a longer period of time promises to distinguish the accuracy between Einstein's ideas and concepts from other scientists.

**Key words:** General Relativity, neutron star, pulsar, double pulsar.

### INTRODUCTION

In a review paper on relativity in 1907 Albert Einstein (1879-1955) presented an equivalence of acceleration and gravity (Einstein, 1907). From this connection, he deduced that gravitation could influence light. In particular, he submitted that light could be bent and also its frequency altered in a gravitational field. However, it was 1911 before he thought these two effects could be detected experimentally near the Sun (Einstein, 1911). Subsequently, during the development of his general theory, he determined, from his equations in 1915, a figure for the anomalous advance of the perihelion of

Mercury (Einstein, 1915). In the following year he doubled his value for the amount of movement of light at the limb of the Sun (Einstein, 1916).

These three outcomes of General Relativity – gravitational deflection, the amount of Mercury perihelion increase and gravitational redshift - became the early classical tests for a new paradigm. The histories of these have been covered by the writer in two previous papers up to the year 1928 (Treschman, 2014a, b). Development after this date depended on improved instrumentation, the arrival of spaceflight and new applications from

E-mail: [treschmankm@bigpond.com](mailto:treschmankm@bigpond.com), Tel: 61-7-38562262.

Author(s) agree that this article remain permanently open access under the terms of the [Creative Commons Attribution License 4.0 International License](https://creativecommons.org/licenses/by/4.0/)

different modes of thinking. The period 1928 to the present has been treated by Treschman (2015) under the topics:

- (a) Weak equivalence principle (equivalence of inertial and gravitational mass and gravitational redshift),
- (b) Orbital precession of a body in gravitational fields (the relativistic perihelion advance of the planets, the relativistic periastron advance of binary pulsars, geodetic precession and the Lense-Thirring effect),
- (c) Light propagation in gravitational fields (gravitational optical light deflection, gravitational radio deflection due to the Sun, gravitational lensing, time delay and atomic clocks) and
- (d) Strong gravity implications (Nordtved effect and potential gravitational waves).

The only double pulsar (two pulsars in mutual orbit) discovered to date has provided a series of unique tests for General Relativity and represents, within the uncertainties, the smallest departure from predictions of the Einstein theory. This paper will concentrate on an analysis of data for this topic. This paper traverses the proposal from the neutron in the atom onwards to a forecast that stars could exist that would be composed entirely of neutrons. Pulsars are then investigated. An understanding of them is revealed as a result of classifying them into three groups. While binary pulsars (a pulsar in mutual orbit with an object not a pulsar) are treated, the emphasis is on the only double pulsar yet discovered, PSR J0737-3039 A and B. Observational data on this pair with the Parkes Radio Telescope in Australia in 2003 provide a highly precise test of the General Theory of Relativity. This paper uses published data to investigate what precision can be reached and how well the General Theory is supported by these observations.

## NEUTRON STARS

James Chadwick (1891-1974) is credited with interpreting his experiments on firing protons and alpha particles at different elements in 1932 as evidence for a particle of mass 1 and charge 0, that is, a neutron (Chadwick, 1932). However, his former supervisor, Ernest Rutherford (1871-1937), had proposed the existence of the neutron 12 years earlier. In a lecture Rutherford outlined his radiation experiments to infer the presence in the atom of a very small nucleus surrounded by electrons. He also conjectured there were electrons within the nucleus performing a different role from those outside the nucleus. He suggested that an atom of helium consisted of four hydrogen atoms and two electrons inside giving a charge of +2 and a mass of 4, with two electrons outside. '...it may be possible for an electron to combine much more closely with the H nucleus, forming a kind of neutral

doublet.' (Rutherford, 1920).

Surprisingly, within two years of Chadwick's pronouncement, (Wilhelm Heinrick) Walter Baade (1893-1960) and Fritz Zwicky (1898-1974) hypothesised that 'a *super-nova* [sic] represents a transition of an ordinary star into a body of considerably smaller mass' (Baade and Zwicky, 1934a) and 'a *super-nova* represents the transition of an ordinary star into a neutron star, consisting mainly of neutrons. Such a star may possess a very small radius and an extremely high density'. (Baade and Zwicky, 1934b)

Recent work has attempted to elicit an equation of state for neutron stars. Theoretical models have been proposed for their nature with a view to establishing limits on their masses as well as a link between the mass and radius. A typical  $1.4 M_{\odot}$  (mass of Sun) object would have a radius of approximately 11.5 km (Lattimer, 2012).

## PULSARS

Angular momentum  $L$  is defined as

$$L = I\omega \quad (1)$$

where  $I$  is the moment of inertia and  $\omega$  is the angular velocity. For a sphere

$$I = \frac{2}{5} MR^2 \quad (2)$$

For mass  $M$  and radius  $R$ . Thus,

$$L = \frac{2}{5} MR^2\omega. \quad (3)$$

Since angular momentum is conserved, as the radius of an object, in this case a neutron star, decreases, the angular velocity must increase. Hence, any neutron star with an initial spin was predicted to have a rapid rotation before any such object was even observed.

In addition, since the entity is expected to have a conducting fluid, a magnetic flux ought to exist. At the surface, the flux would be a product of the magnetic field strength  $B$  and the area of the surface. Again, as the neutron star shrinks resulting in a smaller surface area,  $B$  would be expected to increase.

The forecasts of a rapidly spinning, compact object with a high magnetic field became a reality in 1967 with the discovery of the first pulsar (pulsating source of radio) by (Susan) Jocelyn Bell (1943) (Hewish et al., 1968). In 1968, pulsars were connected with the Vela supernova remnant (Large et al., 1968) and the Crab Nebula relic (Staelin et al., 1968). The cause of the regular and rapid pulses had three possibilities: binary stars, pulsating stars or rotating stars. In 1969, Thomas Gold (1920-2004) dispensed with binary stars on the basis that the periods would decrease as energy was lost, contrary to the observed increase; he eliminated pulsating stars on the

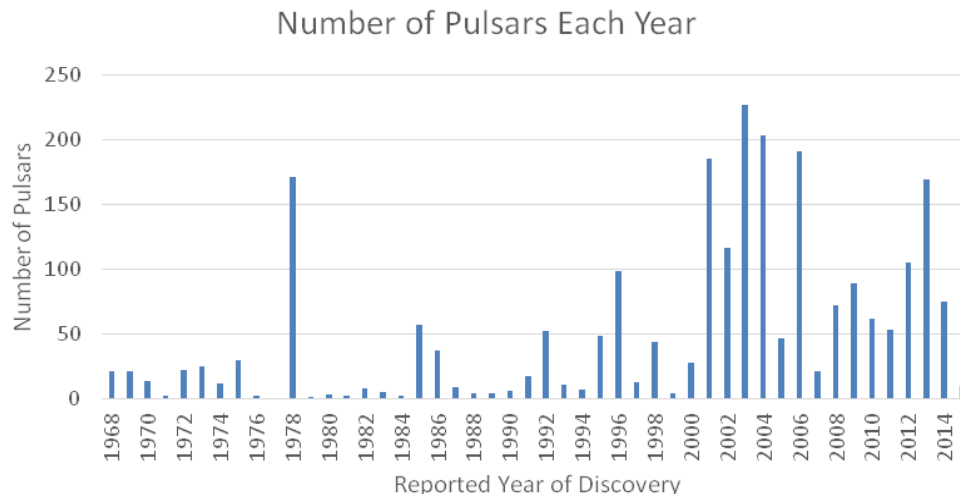


**Figure 1.** Number of pulsars per year of publication with later peaks due to Parkes.

foundation of the length of the period; finally, the rotation rate did not fit a white dwarf as it would fly apart at these speeds, which left, he argued, a rotating neutron star (Gold, 1969).

## PULSAR SURVEYS

Large scale surveys using radio telescopes which led to the discovery of many pulsars have been conducted principally with the 100 m Green Bank Telescope in West Virginia, USA the 305 m Arecibo Observatory in Puerto Rico, the 76 m Jodrell Bank Observatory in England, the two 778 m x 12 m cylindrical paraboloids of the Molonglo Observatory Synthesis Telescope in Australia but more than half of the currently known pulsars have been identified at the 64 m CSIRO (Commonwealth Scientific and Industrial Research Organisation) Parkes Observatory in Australia (Manchester et al., 2005). The proliferation of the number of pulsars detected at Parkes is due, firstly, to the installation in 1997 of a 13 beam receiver. This multibeam pulsar survey commenced in August 1997 with each pointing of the telescope occupying 35 min duration (Manchester, 2001). In the first year of surveillance, each hour of observing time resulted in a new pulsar (Manchester et al., 2001). Secondly, the centre of the Milky Way Galaxy where pulsars are concentrated goes overhead in the Southern Hemisphere. As of May 2015, the Australia Telescope National Facility, that maintains a catalogue for the discoveries from all observatories, had listed 2405 pulsars (ATNF). These are distributed in Figure 1 by the number per year in which they were published. The peak in 1978 is due mainly to a Molonglo survey (Manchester et al., 1978) and the larger numbers in 2001, 2003, 2004, 2006 and 2013 represent surveys published principally from Parkes.

## BINARY PULSARS

While theories were being advanced associating the origin of pulsars with supernovae, another development in the pulsar story was made in 1974 by Russell Alan Hulse (1950) and Joseph Hooton Taylor, Jr (1941). As they conducted a survey at the Arecibo Observatory, they detected the first binary pulsar where a pulsar and another neutron star were in mutual orbit (Hulse and Taylor, 1975). Since then, the total has reached 242 binaries where the companion may be a main sequence star, a neutron star, a white dwarf, a low mass star or another pulsar. These objects orbit each other where the range in period in the ATNF Pulsar Catalogue is from 1.6 h to 23 y.

One of the valuable outcomes from binary pulsars is that the masses of neutron stars may be determined. In a review paper by Lattimer, 33 calculated masses were shown from X-ray – optical, neutron star – neutron star and neutron star – white dwarf binaries. In this selection, the span of masses encompassed 1.00 – 1.700  $M_{\odot}$  (Lattimer, 2012).

## CLASSIFICATION OF PULSARS

In 1982 a very fast rotator was timed at 1.558 ms for one spin (Backer et al., 1982). The term 'millisecond pulsar' was applied and encompassed any pulsar with a period shorter than 10 ms (Bhattacharya and van den Heuvel, 1991). At the other end of the spinning scale, a seemingly different type of object with pulses of 5.54 s was uncovered with the Parkes radio telescope in 2006 (Camilo et al., 2006). It was actually connected with a burst of X-rays previously detected by spacecraft in 2003. This class contains the so called magnetars and comprises anomalous X-ray pulsars and gamma ray bursters.

## Number of Pulsars versus Period > 1 s

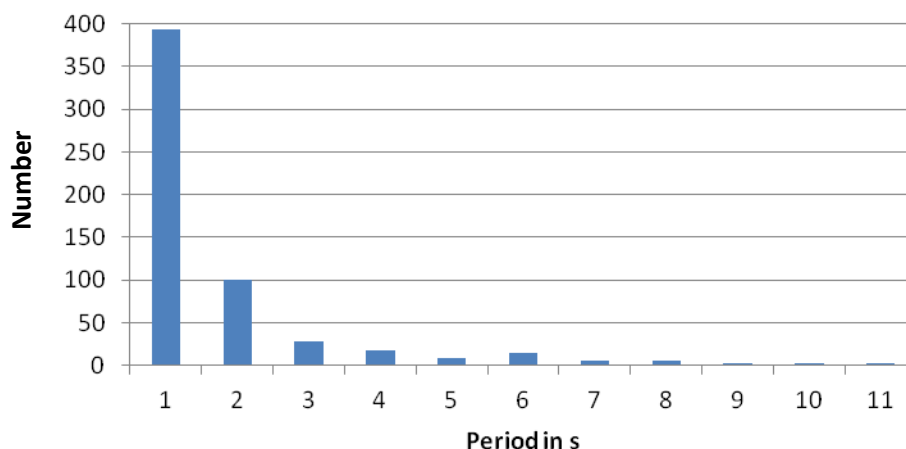


Figure 2. Number of pulsars with periods 1-12 s.

## Number of Pulsars versus Period < 1 s

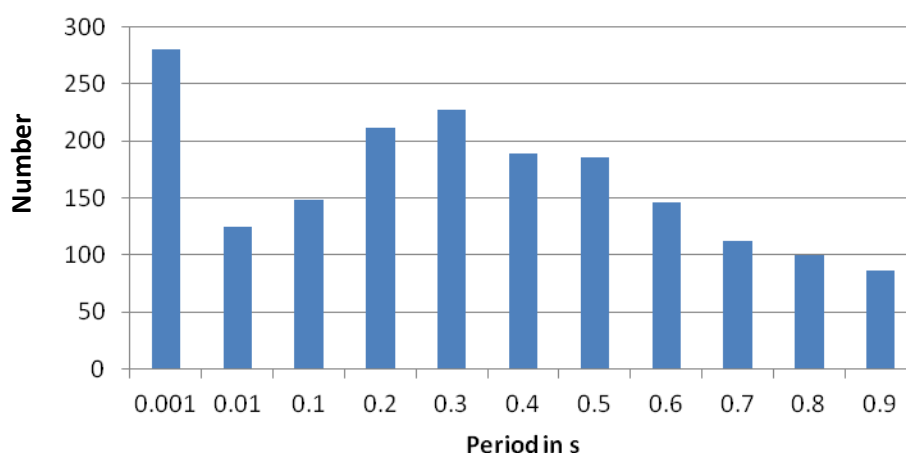


Figure 3. Number of pulsars with periods < 1 s.

From the ATNF catalogue of all known pulsars, the one with the slowest spin has a period  $P$  of 11.8 s and the fastest 1.4 ms, that is, over 700 times per second. Of the 2405 pulsars that have been logged, 2392 have their measured period displayed. The 581 with a period > 1 s are exhibited in Figure 2 where 1 s refers to the duration > 1 s but < 2 s and so on. For the 1811 pulsars with periods < 1 s, 1406 have a spin > 0.1 s. From an analysis of 815 pulsars, it has been estimated that perhaps 40% are born in the range 0.1 to 0.5 s (Vranesevic et al., 2004). Thus, the region 0.1 to 1.0 s has been further subdivided into 0.1 s lots as in Figure 3.

*“The pulse period is very predictable, but it is not constant. ... Pulsars are powered by the kinetic energy of*

*rotation. They steadily lose energy, mainly in the form of a high-energy wind of charged particles and magnetic-dipole radiation, that is, electromagnetic waves at the neutron star’s rotation frequency (Manchester, 2001)”.*

The measure of this loss of energy may be gauged in the slowdown rate of the period,  $\dot{P}$  in  $\text{s s}^{-1}$ . An interesting pattern emerges if the logarithm of  $\dot{P}$  is graphed against the logarithm of  $P$ . The plots in Figure 4 are produced from within the ATNF catalogue but here have been teased apart into the majority of pulsars, the high energy ones and the binaries respectively from left to right. The product of  $P$  and  $\dot{P}$  leads to a measure of the magnetic field at the surface  $B_S$  as in the formula:



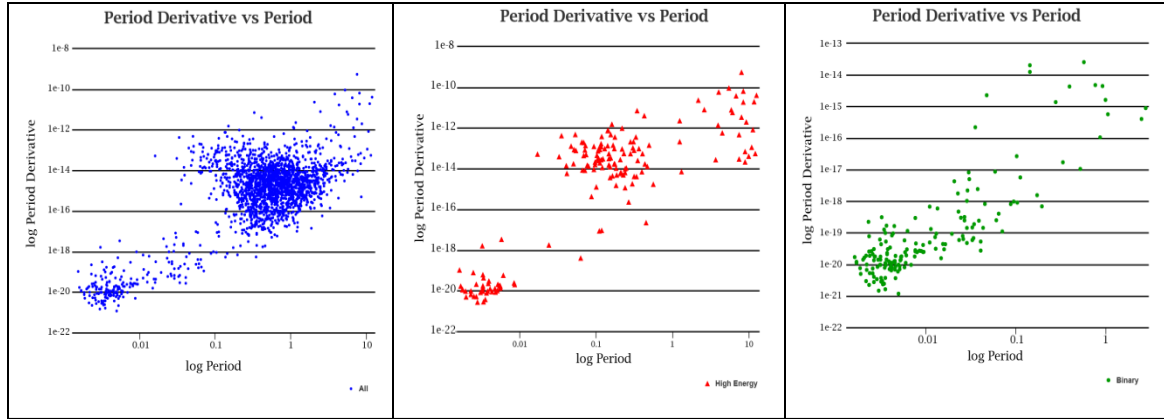


**Figure 4.** Log of change of period per s versus log of period for, from left, most pulsars, high energy pulsars, binaries. Note that the vertical axes are identical but the horizontal scale for the binaries is different from that of the other two.

$$B_S = (3c^2/8\pi^2 R^6 P\dot{P})^{0.5} \text{ in G (gauss)} \quad (4)$$

$\approx 3.2 \times 10^{19} (P\dot{P})^{0.5}$  G for  $I \approx 10^{38}$  kg m<sup>2</sup> and  $R \approx 10^4$  m (Bhattacharya and van den Heuvel, 1991). For a typical high energy pulsar in the centre panel of Figure 4,  $10^{19} \times (10^{-1} \text{ s} \times 10^{-13} \text{ s s}^{-1})^{0.5} \approx 10^{12}$  G. From the surface magnetic field data in the ATNF catalogue, the highest is given as  $2.22 \times 10^{14}$  G. This region embodies the magnetars which have large magnetic fields, slower rotations but faster rates of loss of energy. Also, the loss is not always uniform and is often in the form of bursts of X-rays or gamma rays. The decay of  $B$  powers the emission of radiation predominately in the high energy end of the spectrum. The bursts are believed to be connected with two different situations: the collapse of a star and the merger of neutron stars. From the left panel of Figure 4, a central pulsar at  $10^{-1}$  s and change at  $10^{-15}$  s s<sup>-1</sup> has  $B_S \approx 10^{11}$  G from Equation (4). They are faster rotators, have medium magnetic fields but lose their energy more slowly than the magnetars. In contrast, the binaries in the right panel of Figure 4 would have a typical result of  $10^{-2}$  s, loss at  $10^{-20}$  s s<sup>-1</sup> for  $B_S \approx 10^8$  G. The lowest value in the catalogue is  $3.21 \times 10^7$  G. These binary pulsars are fast rotators, most reside in the millisecond class, have lower magnetic fields by comparison and lose their energy much more slowly. More than half of them have been detected in globular clusters (D'Amico et al., 2003). Their scenario is that they were older, slow rotators and even though they probably also formed from supernovae, each possessed a companion which was not ejected by this mammoth event. As the companion evolved, some of its matter accreted to the other member. The rise in angular momentum led to an increase in rotation rate of what effectively became a recycled pulsar (Possenti et al., 2004).

## DOUBLE PULSAR

Where the term binary pulsar is applied to a pulsar and a companion other than another pulsar, the term double pulsar is used for two pulsars in mutual orbit. The only double pulsar system discovered to date is PSR J0737-3039A and PSR J037-3039B in the constellation Puppis, referred hereafter as A and B. The data for A were collected by Marta Burgay (1976) in April 2003 at Parkes and processed at Jodrell Bank (Burgay et al., 2003). In October of the same year, Duncan Ross Lorimer (1969) was testing code at Parkes on the data of Burgay and identified a second pulsar which was not detectable in the original records as B was only strong for two short intervals each orbit (Possenti et al., 2004). The saga is articulately presented in chapter 14 of McNamara's book on pulsars (McNamara, 2008). It was decided by the parties involved (Sarkissian, 2014) that as Burgay had already submitted for publication, it would be followed later by Andrew Lyne as principal author who was supervising Burgay (Lyne et al., 2004). Some of the physical parameters of the double pulsar are displayed in Table 1. The digit/s in parentheses following the measurement refer/s to the uncertainty in the last digit/s.

There are five orbital parameters, known as Keplerian parameters, which are required to reference the time of arrival of pulses to the barycentre of the binary system (Kramer, 2004). They are based on Newton's laws of motion and his law of universal gravitation and are calculated as an isolated two-body situation. These are shown in Table 2.

However, changes do arise due, in some situations, to the presence of other masses and, in the case of the double pulsar, to the effects of relativity. Departures from the Keplerian descriptions are referred to as post-Keplerian parameters (PKPs). Stairs explains: "*The tests of GR [General Relativity] that are possible through pulsar timing fall into two broad categories: setting limits*

**Table 1.** Some physical parameters of the double pulsar (Kramer, 2006a).

Physical parameter	Values
right ascension	07 <sup>h</sup> 37 <sup>m</sup> 51 <sup>s</sup> .249 27(3)
declination	-30°39'40".719 5(5)
spin frequency A	44.054 069 392 744(2) s <sup>-1</sup>
spin frequency B	0.360 560 355 06(1) s <sup>-1</sup>
inclination <i>i</i>	88°.69(-76, +50)

**Table 2.** Keplerian parameters of the double pulsar (Kramer et al., 2006a).

Parameter	Pulsar A	Pulsar B
orbital period $P_b$	0.102 251 562 48(5) d	
eccentricity <i>e</i>	0.087 777 5(9)	-
projected semi-major axis $x = a/c \sin i$ for <i>a</i> , semi-major axis	1.415 032(1) s	1.516 1(16) s
longitude of periastron from the ascending node $\omega$	87°.033 1(8)	87°.033 1 + 180°.0
the epoch of periastron passage (MJD)	53 156.0	

on the magnitudes of the parameters that describe violations of equivalence principles, often using an ensemble of pulsars, and verifying that the measured post-Keplerian timing parameters of a given binary system match the predictions of strong-field GR better than those of other theories (Stairs, 2003)".

Measurements are performed on the time of arrival of the pulse energy. As this signal travels through interstellar space, the presence of electrons along the path interferes differently with the frequencies so that the higher the frequency the earlier the arrival. The pulse dispersion is thus an approximate measure of distance. 'The observational parameters ... are obtained from a least-squares solution of the arrival-time data ...' (Will, 2006).

## ANALYSES OF DOUBLE PULSAR PARAMETERS

Stairs lists the following five equations of PKP in terms of the stellar masses (Stairs, 2003).

$$\dot{\omega} = 3 (P_b/2\pi)^{-5/3} (T_O M)^{2/3} (1 - e^2)^{-1} \quad (5)$$

$$Y = e(P_b/2\pi)^{1/3} T_O^{2/3} M^{4/3} M_B(M_A + 2M_B) \quad (6)$$

$$\dot{P}_b = -192\pi/5 (P_b/2\pi)^{-5/3} (1 + 73/24 e^2 + 37/96 e^4)(1 - e^2)^{-7/2} T_O^{5/3} M_A M_B M^{-1/3} \quad (7)$$

$$r = T_O M_B \quad (8)$$

$$s = x(P_b/2\pi)^{-2/3} T_O^{-1/3} M^{2/3} M_B^{-1} \quad (9)$$

The symbol  $T_O$  stands for the time for light to cross the radius of the Sun and is a term that allows the resultant pulsar masses to be given in terms of  $M_O$ .  $T_O = GM_O/c^3 = 6.673 \times 10^{-11} \text{ N m}^2 \text{ kg}^{-2} \times 1.989 \times 10^{30} \text{ kg} / (2.997 \times 10^8 \text{ m s}^{-1})^3 = 4.926 \times 10^{-6} \text{ s}$ . This compares closely with the literature value of  $4.925 \times 10^{-6} \text{ s}$ .  $x$  is the projected semi-major axis of the binary orbit.

In Equation (5),  $\dot{\omega}$  is the time rate of change of the longitude of periastron from the ascending node. It is the relativistic advance of periastron and is analogous to the relativistic perihelion advance of Mercury (or any other planet) in the solar system. This equation may be rearranged to provide a solution for  $M$ , the mass of the system which equals the sum of the individual masses  $M_A + M_B$ .

$$M = [\dot{\omega}/3 (P_b/2\pi)^{5/3} T_O^{-2/3} (1 - e^2)]^{3/2} \quad (10)$$

Since  $\dot{\omega} = 16.899 \text{ } 47^\circ \text{ yr}^{-1}$ , it needs to be changed into radian s<sup>-1</sup>, and  $P_b$  to s. This resultant value and subsequent ones are taken from Kramer et al. (2006a).  $M = 2.587 \text{ } 08(16) M_O$ . Thus,

$$M_A + M_B = 2.587 \text{ } 08 \text{ or } M_B = -M_A + 2.587 \text{ } 08. \quad (11)$$

A graph of  $M_B$  versus  $M_A$  may then be drawn. As further PKPs are derived in terms of masses, these are added as graphs on the original plot. The intersection gives specific values for the masses of A and B. General Relativity may then be judged as to how constrained the quantities of the masses are. This method has an appeal

**Table 3.** Post-Keplerian parameters and other results of the double pulsar (Kramer, 2006a).

Parameter	Value	Equation
advance of periastron $\dot{\omega}$	16.899 47(68) ° yr <sup>-1</sup>	5
gravitational redshift $Y$	0.385 6(26) x 10 <sup>-3</sup> s	6
orbital period derivative $\dot{P}_b$	-1.252(17) x 10 <sup>-12</sup> s s <sup>-1</sup>	7
Shapiro delay $r$	6.21(33) x 10 <sup>-6</sup> s	8
Shapiro delay $s$	0.999 74(-39,+16)	9
mass of system	2.587 08(16) M <sub>⊙</sub>	
mass of A	1.338 1(7) M <sub>⊙</sub>	
mass of B	1.248 9 M <sub>⊙</sub>	
mass ratio	1.071 4(11)	
distance based on dispersion measure	≈ 500 pc (10 <sup>20</sup> m)	

visually. Alternatively, two equations give two unknowns of the masses which may be solved mathematically. Then, further parameters are derived from the masses and the difference between the new parameter and its observational value provides a percentage variation for the theory of General Relativity.

Equation (6) contains the gravitational redshift parameter  $Y$  and is a combination of time delay and gravitational redshift. The frequency change is predicted by Einstein in that time runs differently in the region of a mass and a volume somewhat removed. It corresponds to the average amplitude of delays in arrival time due to changes in speed of the pulsars and the distance between them as they traverse their elliptical orbit. For the measured  $Y = 0.385\ 6(26) \times 10^{-3}$  s, Equations (5) and (6) yield

$$M_A = 1.338\ 1(7) M_{\odot} \text{ and } M_B = 1.248\ 9 M_{\odot}.$$

The time derivative of the orbital period change  $\dot{P}_b$  is caused by gravitational wave damping. Equation (7) produces a result of  $-1.252(17) \times 10^{-12}$  s s<sup>-1</sup>. Due to the fortuitous circumstance of the double system being almost edge on to the line of sight, the two parameters representing the Shapiro delay may also be determined (Kramer et al., 2006b). From Equation (8) the Shapiro delay  $r$  due to the medium of transmission is calculated as  $6.21(33) \times 10^{-6}$  s. In reverse, it is the range of the Shapiro delay that provides an estimate of the companion mass as the signal from A passes through the spacetime of B (van Straten et al., 2001).

To conclude the calculations of the PKPs, Equation (9) derives the shape of the Shapiro delay  $s \equiv \sin i$  (Burgay et al., 2005) as  $0.999\ 74(-39, +16)$ . A further parameter which is possible with the double pulsar is to obtain a mass ratio  $R$  of the components by measuring the semi-major axes  $a$  of the elliptical orbits from the equality in the following subsequent equation.

$$R = M_A/M_B = a_B/a_A \quad (12)$$

This gives  $1.071\ 4(11)$ . The measurements of the PKPs from Equations (5) to (9) and data on masses and distance are summarised in Table 3. The advance of the

periastron  $\dot{\omega}$  has been measured to a precision approaching  $10^{-5}$ . If this and  $R$  are used to solve for  $M_A$  and  $M_B$ , the values of the other four PKPs mentioned here may be calculated. This then gives tests of General Relativity as shown in Table 4 (Kramer et al., 2006a).

Departures from General Relativity are calculated here as the uncertainty in the ratio of 1.0 as a percentage. For example, for  $s$  the uncertainty is  $0.000\ 50$  which is  $0.05\%$ .

Hence, differences from GR are  $1.4\%$  for  $\dot{P}_b$ ,  $0.68\%$  for  $Y$ ,  $5.5\%$  for  $r$  and  $0.05\%$  for  $s$ . This result for  $s$  is the most precise test ever of any technique used for

comparison with Einstein's theory. The parameters  $\dot{\omega}$ ,  $Y$ ,  $r$  and  $s$  were obtained within seven months of observation. This level of precision of  $\dot{P}_b$  followed 2.5 years of timing.

## FURTHER DATA

The distance datum based on the dispersion measure is claimed to be in error by a factor of two. With measurements between 2006-2008 of the annual geometric parallax with the Australian Long Baseline Array, the figure has been given as  $1\ 150 (+220, -160)$  pc (Deller et al., 2009). From the separation between the

pulsars of  $8 \times 10^8$  m, the precision of  $\dot{P}_b$  is such as to be able to deduce a decreasing separation between the pulsars of  $7\ \text{mm}\ \text{d}^{-1}$  (Kramer et al., 2006a). After 10 more years of timing, this parameter may reach the  $0.01\%$  level.

**Table 4.** PKP comparisons of observed and GR predictions for the double pulsar.

PKP	observed value	GR value	ratio observed/GR
$\dot{P}_b \text{ s s}^{-1}$	1.252(17)	1.247 87(13)	1.003(14)
$Y \times 10^{-3} \text{ s}$	0.385 6(26)	0.384 18(22)	1.003 6(68)
$r \times 10^{-6} \text{ s}$	6.21(33)	6.153(26)	1.009(55)
s	0.999 74(-39,+16)	0.999 87(-48,+13)	0.999 87(50)

The supernova which caused the two pulsars did not throw the binary system apart but would be expected to result in a misalignment between the pulsar spin axes and their orbital axis. Geodetic precession would lead to relativistic spin-orbit coupling so that the pulsar spin axes would precess about the total angular momentum axis (Kramer, 2004; Manchester, 2010). The angular frequency period  $\Omega_p$  for this is embedded in the relationship

$$\Omega_p = \frac{1}{2} (P_b/2\pi)^{-5/3} T_O^{2/3} M_B(4M_A + 3M_B)/(1 - e^2)M^{4/3}. \quad (13)$$

The calculated period for pulsar B around the total orbital angular momentum axis is 70.95 year (Manchester, 2015a).  $360^\circ/70.95 \text{ yr} = 5^\circ.074 \text{ yr}^{-1}$ . Within an uncertainty of 13%, the precessional rate obtained of  $4^\circ.77 (+0.66, -0.65) \text{ yr}^{-1}$  is consistent with a General Relativity prediction of  $5^\circ.073 4 \pm 0^\circ.000 7 \text{ yr}^{-1}$  (Breton et al., 2008). From a study of eclipses of pulsar A by the magnetosphere of pulsar B, it has been inferred that the inclination of the rotation axis of pulsar B to the normal of the orbital plane is  $\approx 60^\circ$  and its angle to the magnetic axis  $75^\circ$  (Lyutikov and Thompson, 2005). Pulse profile analysis points to  $\approx 90^\circ$  for the difference between the spin and magnetic axes of pulsar A but only  $3^\circ.2$  difference between its spin and orbital angular momentum axes (Ferdman et al., 2013). As a result, no secular change has been pursued for a measurement of the precessional period of pulsar A. Some further data given in Table 5 (Lyne et al., 2004), on the rotational periods  $P$  of pulsars A and B together with

their time rates of change  $\dot{P}$  may be used to calculate their surface magnetic fields and time rate of energy loss  $\dot{E}$ .

From Equation (4),  $B_A = 6.3 \times 10^9 \text{ G}$  and  $B_B = 1.2 \times 10^{12} \text{ G}$  (Yuen et al., 2012). Also,

$$\dot{E} = -4\pi^2 I \dot{P} / P^3. \quad (\text{Manchester, 2001}) \quad (14)$$

$\dot{E}_A = 5.9 \times 10^{26} \text{ W}$  and  $\dot{E}_B = 1.6 \times 10^{23} \text{ W}$  where  $1 \text{ W} \equiv 10^7 \text{ erg s}^{-1}$  (Yuen et al., 2012). Some concept of the dense nature of a pulsar may be gauged by comparison with the atomic nucleus. With the masses of pulsar A and

**Table 5.** Parameters for spin periods and their time rates of change.

Parameter	Observed value
$P_A$	0.022 699 378 556 15(6) s
$\dot{P}_A$	$1.74(5) \times 10^{-18} \text{ s s}^{-1}$
$P_B$	2.773 460 747 4(4) s
$\dot{P}_B$	$0.88(13) \times 10^{-15} \text{ s s}^{-1}$

a neutron being respectively  $1.338 1 M_\odot$  and  $1.674 928 6 \times 10^{-27} \text{ kg}$ , on the assumption that pulsar A were comprised totally of neutrons, there would be of the order of  $10^{57}$  neutrons present. The density of pulsar A, taking the radius as  $1.15 \times 10^4 \text{ m}$ , would be  $4.2 \times 10^{17} \text{ kg m}^{-3}$  compared with that of an atomic nucleus of  $2.3 \times 10^{17} \text{ kg m}^{-3}$ . The designation neutron star is truly appropriate.

## FUTURE

As a result of the dynamic changes in the double pulsar system PSR J0737-3039A/B, the beam of pulsar B ceased sweeping across Earth in 2008. However, it is expected to again intersect Earth in the near future (Manchester, 2015b). The longer the time span of observations, the more precise the measurements of this system become. This places tighter constraints on the parameters and provides a more stringent test of General Relativity or competing theories.

Radio receivers are the instruments which provide accurate measurement of timing for pulsars. Nevertheless, other realms of the electromagnetic spectrum may elucidate data that give a more detailed picture of the operation of the double pulsar. In 2006, the Chandra X-ray Observatory collected data on the system at this high energy end and the interpretation was that it showed that the emission was due to the shock from pulsar A interacting with the interstellar medium (Granot and Mészáros, 2004). Later, in 2012, the Hubble Space Telescope acquired images in the far ultraviolet region (Durant et al., 2014).

A 500 m radio telescope is slated for first light in China

in 2016. A stated objective of this project is an emphasis on collecting information on more distant pulsars (Nan et al., 2011). When the Square Kilometre Array begins its operation, it also has targeted pulsar surveys with an emphasis on the millisecond variety (Carilli and Rawlings, 2004) with improved timing precision (Shao et al., 2014).

As a larger collection of pulsar, binary pulsar and double pulsar samples increases, measurements of moments of inertia will allow a deeper insight into the nature of superdense matter (Kramer et al., 2006a).

One of the pursuits in pulsar investigation is the detection of gravitational waves which are predicted by General Relativity. The amount of release of energy is consistent with the theory but the instrumentation available today is not sensitive enough to detect and measure it. When a figure was forthcoming for the merger rate of the double pulsar of  $85 \times 10^6$  yr (Burgay, 2011), the expected rate of binary pulsar collisions increased dramatically. This gave greater impetus to the likelihood of detecting this far greater amount of energy. The Laser Interferometric Gravitational-Wave Observatory (LIGO) in the United States of America, the Japanese TAMA project, German-British GEO detector in Germany and the European Gravitational Observatory in Italy have embarked on the quest to discovery such a phenomenon (Abbott et al., 2009).

This prominence given to increasing the precision of measurements is not just about discriminating between rival theories for understanding the Universe. General Relativity has passed with flying colours any test thrown at it. However, it started in 1915 as a theoretical construct without any experimental support. Scientists “*did not dream that transition to a relativistic system would have observational consequences* (Kuhn, 1962, 2012)”. The situation morphed when it was realised that there were three ‘classical’ predictions upon which its mettle could be judged. Even then, the field was quite dormant. Interest was piqued 50 years after the formulation of the theory as new thinking was applied, instrumentation progressed, the space era had begun and more exotic objects started presenting themselves in the cosmos. Up to this point, it could be seen that Newton’s laws could still be applied with Einstein filling in when speeds increased into the regime of the speed of light or masses became somewhat larger than that of the Sun. However, the application of General Relativity in the confines of the solar system, known as the weak field situation, completely trumps Newtonian theory in the strong fields of, for example, pulsars. A paradigm shift ensued. Where might General Relativity lead us? Just as the extent of its applicability was not predictable, the theory needs to be mined for what else it may elucidate. As one sign of the dramatic change, one may look at a criterion for a paradigm shift in conferences held specifically in a field. The first international convocation completely devoted to General Relativity was in 1955, a few months subsequent to Einstein’s death. These are now held each three years,

with 21 having occurred. Now, at the 100 year anniversary of General Relativity, the field is still providing promise for many scientists.

## CONCLUSION

The prediction of superdense forms of matter predated the recognition of neutron stars. With the arrival on the scene of pulsars in 1967, an entire new field emerged and General Relativity was the guiding post to scientific understanding. Entering the scene in 1974, binary pulsars extended the possibilities and precision of measurement. In 2003, the discovery of a double pulsar has provided scientists with a unique gamut of prospects in the strong field arena. Astronomical tests of General Relativity have included inertial and gravitational equivalence, gravitational redshift, relativistic perihelion and periastron advance, geodetic precession, light propagation in gravitational fields and implications in strong gravity regimes. Of all of these, the most accurate figure to date of 0.05% for the departure between observation and General Relativity comes from a parameter of the double pulsar PSR J037-3039A/B.

## Conflict of Interest

The authors have not declared any conflict of interest.

## ACKNOWLEDGEMENTS


Two members of the team involved in the discovery of the double pulsar have been most helpful. Dr John Sarkissian, Operations Scientist at the Parkes Radio Telescope, gave me, per telephone, background to the discovery of the double pulsar and the decisions made by a number of members of the group. Dr Dick Manchester, a CSIRO Fellow provided time for me in my visit to the Sydney arm of the Parkes radio telescope where he answered my questions on the techniques involved in pulsar measurement. Subsequently, he has responded to a number of queries I had in my understanding of facets of the double pulsar measurements.

This paper forms part of my PhD dissertation at the University of Southern Queensland. My supervisors, Dr Brad Carter and Dr Nick Lomb, have provided feedback on my written work, including recommendations for improved communication of some ideas.

## REFERENCES

- Abbott BP et al (2009). “LIGO: The Laser Interferometer Gravitational-Wave Observatory” Reports on Progress in Physics [arXiv:0711.3041](https://arxiv.org/abs/0711.3041):1-50.  
Australia Telescope National Facility Pulsar Catalogue <http://www.atnf.csiro.au>.

- Baade W, Zwicky F (1934a). On super-novae. *Proceedings National Academy Sci.* 20(5):254-259.
- Baade W, Zwicky F (1934b). Cosmic rays from super-novae. *Proceedings National Academy Sci.* 20(5):259-263.
- Backer DC, Kulkarni SR, Heiles C, Davis MM, Goss WM (1982). "A millisecond pulsar". *Nature* 300:615-618.
- Bhattacharya D, van den Heuvel EPJ (1991). Formation and evolution of binary and millisecond pulsars. *Phys. Lett.* 203(1- 2):1-124.
- Breton RP, Kaspi VM, Kramer M, McLaughlin MA, Lyutikov M, Ransom SM, Stairs IH, Ferdman RD, Camilo F, Possenti A (2008). Relativistic spin precession in the double pulsar. *Science* 321:104-107.
- Burgay M, D'Amico N, Possenti A, Manchester RN, Lyne AG, Joshi BC, McLaughlin MA, Kramer M, Sarkissian JM, Camilo F, Kalogera V, Kim C, Lorimer DR (2003). An increased estimate of the merger rate of double neutron stars from observations of a highly relativistic system. *Nature* 426:531-533.
- Burgay M, D'Amico N, Possenti A, Manchester RN, Lyne AG, Joshi BC, McLaughlin MA, Kramer M, Sarkissian JM, Camilo F, Kalogera V, Kim C, Lorimer DR (2005). The highly relativistic binary pulsar PSR J0737-3039A: discovery and implications. *ASP Conf. Series* 328:53-58.
- Burgay M (2011). The double pulsar system in its 8<sup>th</sup> anniversary. *Science with Parkes @ 50 Years Young.*
- Camilo F, Ransom SM, Halpern JP, Reynolds J, Helfand DJ, Zimmerman N, Sarkissian J (2006). Transient pulsed radio emission from a magnetar. *Nature* 442:892-895.
- Carilli CL, Rawlings S (2004). Science with the square kilometer array: motivation, key science projects, standards and assumptions. [arXiv: astro-ph/0409274](https://arxiv.org/abs/astro-ph/0409274).
- Chadwick J (1932). Possible existence of a neutron. *Nature* 129:312.
- D'Amico N, Possenti A, Manchester RN, Lyne AG, Camilo F, Sarkissian J (2003). Searching for millisecond pulsars in globular clusters at Parkes. *Astron. Soc. Pacific Conf. Series* 302:375-379.
- Deller AT, Bailes M, Tingay SJ (2009). Implications of a VLBI distance to the double pulsar J0737-3039A/B. *Science* [arXiv:0902.0996](https://arxiv.org/abs/0902.0996).
- Durant M, Kargaltsev O, Pavlov GG (2014). Hubble Space Telescope detection of the double pulsar system J0737-3039 in the far-ultraviolet. *Astrophys. J.* 783(1):L22-L26.
- Einstein A (1907). On the relativity principle and the conclusions drawn from it. *Jahrbuch der Radioaktivität und Elektronik.* 4:411-462.
- Einstein A (1911). On the influence of gravitation on the propagation of light. *Annalen der Physik* 35:898-908.
- Einstein A (1915). Explanation of the perihelion motion of mercury from the general theory of relativity. *Preußische Akademie der Wissenschaften (Prussian Academy of Sciences).* 6(21):831-839.
- Einstein A (1916). The foundations of the general theory of relativity. *Annalen der Physik.* 49:769-822.
- Ferdman RD, Stairs IH, Kramer M, Breton RP, McLaughlin MA, Freire PCC, Possenti A, Stappers BW, Kaspi VM, Manchester RN, Lyne AG (2013). The double pulsar: evidence for neutron star formation without an iron core-collapse supernova. *Astrophys. J.* 767 (85):1-11.
- Gold T (1969). Rotating neutron stars and the nature of pulsars. *Nature* 222(5175):25-27.
- Granot J, Mészáros P (2004). High energy emission from the double pulsar system J0737-3039. *Astrophys. J.* 609:L17-L20.
- Hewish A, Bell SJ, Pilkington JDH, Scott PF, Collins RA (1968). Observation of a rapidly pulsating radio source. *Nature* 217:709-713.
- Hulse RA, Taylor JH (1975). Discovery of a pulsar in a binary system. *Astrophys. J.* 195:L51-53.
- Kramer M (2004). General relativity with double pulsars. *SLAC Summer Institute on Particle Phys. (SSI04):*1-14.
- Kramer M, Stairs IH, Manchester RN, McLaughlin MA, Lyne AG, Ferdman RD, Burgay M, Lorimer DR, Possenti A, D'Amico N, Sarkissian JM, Hobbs GB, Reynolds JE, Freire PCC, Camilo F (2006a). Tests of general relativity from timing the double pulsar. *Science* 314(97):97-102.
- Kramer M, Stairs IH, Manchester RN, McLaughlin MA, Lyne AG, Ferdman RD, Burgay M, Lorimer DR, Possenti A, D'Amico N, Sarkissian J, Joshi BC, Freire PCC, Camilo F (2006b). Strong-field tests of gravity with the double pulsar. *Annalen der Physik.* 15(1-2):34-42.
- Kuhn TS (1962, 2012 edition). *The structure of scientific revolutions.* University of Chicago Press.
- Large MI, Vaughan AE, Mills BY (1968). A pulsar supernova association? *Nature* 20(5165):340.
- Lattimer JM (2012). The nuclear equation of state and neutron masses. *Ann. Rev. Nuclear Particle Sci.* 62:485-515.
- Lyne AG, Burgay M, Kramer M, Possenti A, Manchester RN, Camilo F, McLaughlin MA, Lorimer DR, D'Amico N, Joshi BC, Reynolds JE, Freire PCC (2004). A double-pulsar system: a rare laboratory for relativistic gravity and plasma physics. *Science* 303:1153-1157.
- Lyutikov M, Thompson C (2005). Magnetospheric eclipses in the double pulsar system PSR J0737-3039. *Astrophys. J.* 634:1223-1241.
- McNamara G (2008). *Clocks in the sky – the story of pulsars*, Springer.
- Manchester RN, Lyne AG, Taylor JH, Durdin JM, Large MI, Little AG (1978). The second Molonglo pulsar survey – discovery of 155 pulsars. *Monthly Notices Royal Astron. Soc.* 185:409-421.
- Manchester RN (2001). "Finding pulsars at Parkes". *Publ. Astron. Soc. Australia.* 18:1-11.
- Manchester RN, Lyne AG, Camilo F, Bell JF, Kaspi VM, D'Amico N, McKay NPF, Crawford F, Stairs IH, Possenti A, Kramer M, Sheppard DC (2001). The Parkes multi-beam survey – I. observing and data analysis systems, discovery and timing of 100 pulsars. *Monthly Notices Royal Astron. Soc.* 328:17-35.
- Manchester RN, Hobbs GB, Teoh A, Hobbs M (2005). The Australia Telescope National Facility Pulsar Catalogue. *Astronol. J.* 129:1993-2006.
- Manchester RN, Kramer M, Stairs IH, Burgay M, Camilo F, Hobbs GB, Lorimer DR, Lyne AG, McLaughlin MA, McPhee CA, Possenti A, Reynolds JE, van Straten W (2010). Observations and modeling of relativistic spin precession in PSR J1141-6545. *Astrophys. J.* 710:1694-1709.
- Manchester RN (2015a). Pulsars and gravity. *Int. J. Modern Phys. D.* 24. [arXiv:1502.05474](https://arxiv.org/abs/1502.05474).
- Manchester RN (2015b). Personal conversation in Sydney.
- Nan R, Li D, Jin C, Wang Q, Zhu L, Zhu W, Zhang H, Yue Y, Qian L (2011). The five-hundred-meter aperture spherical radio telescope (FAST) project. *Int. J. Phys. D:*1-36.
- Possenti A, Burgay M, D'Amico N, Lyne AG, Kramer M, Manchester RN, Camilo F, McLaughlin MA, Lorimer D, Joshi BC, Sarkissian JM, Freire PCC (2004). The double-pulsar PSR J0737-3039A/B. *Memorie della Società Astronomica Italiana. Supplementi.* 5:142-147.
- Rutherford E (1920). Nuclear constitution of atoms. *Bakesian Lecture, Proc. Roy. Soc. London.* 97(686):374-400.
- Sarkissian J (2014). Telephone conversation.
- Shao L, Stairs IH, Antoniadis J, Deller AT, Freire PCC, Hessels JWT, Janssen GH, Kramer M, Kunz J, Lämmerzahl C, Perlick V, Possenti A, Ransom S, Stappers BW, van Straten W (2014). Testing gravity with pulsars in the SKA era. *Proceed. Sci.* [arXiv:1501.00058](https://arxiv.org/abs/1501.00058):1-20.
- Staelin DH, Reifenstein III, Edward C (1968). Pulsating radio sources near the Crab Nebula. *Science* 162(3861):1481-1483.
- Stairs IH (2003). Testing general relativity with pulsar timing. *Living Rev. Relativ.* 6:5-49.
- Treschman KJ (2014a). Early astronomical tests of general relativity: the gravitational deflection of light. *Asian J. Phys.* 23(1- 2):145-170.
- Treschman KJ (2014b). Early astronomical tests of general relativity: the anomalous advance in the perihelion of mercury and gravitational redshift. *Asian J. Phys.* 23(1- 2):171-188.
- Treschman KJ (2015). Recent astronomical tests of general relativity. *IJPS* 10(2):90-105.
- van Straten W, Bailes M, Britton MC, Kulkarni SR, Anderson SB, Manchester RN, Sarkissian J (2001). A test of general relativity from the three-dimensional orbital geometry of a binary pulsar. *Nature* 412:158-160.
- Vranesevic N, Manchester RN, Lorimer DR, Hobbs GB, Lyne AG, Kramer M, Camilo F, Stairs IH, Kaspi VM, D'Amico N, Possenti A, Crawford F, Faulkner AJ, McLaughlin MA (2004). Pulsar birthrates from the Parkes multibeam survey. *Astrophys. J.* 617:L139-L142.
- Will CW (2006). The confrontation between general relativity and experiment. *Living Rev. Relativ.* 9:1-100.
- Yuen R, Manchester RN, Burgay M, Camilo F, Kramer M, Melrose DB, Stairs IH (2012). Changes in polarization position angle across the eclipse in the double pulsar system. *Astrophys. J.* 752:L32-L36.

A close-up photograph of a microscope with a blue background. The microscope is the central focus, with its objective lenses and eyepiece visible. The background is a soft, out-of-focus blue, suggesting a laboratory setting. The text is overlaid on a semi-transparent grey rectangular area in the upper half of the image.

# International Journal of Physical Sciences

## Related Journals Published by Academic Journals

- *African Journal of Pure and Applied Chemistry*
- *Journal of Internet and Information Systems*
- *Journal of Geology and Mining Research*
- *Journal of Oceanography and Marine Science*
- *Journal of Environmental Chemistry and Ecotoxicology*
- *Journal of Petroleum Technology and Alternative Fuels*

**academicJournals**